UNIVERSITÀ DEGLI STUDI DI SALERNO

Dipartimento di Ingegneria Civile

Dottorato di Ricerca

in

Rischio e Sostenibilità nei sistemi dell'Ingegneria civile, edile e ambientale"

Curriculum in *Ingegneria delle strutture*

XXXI Ciclo N.S. (2015-2018)

CONTINUUM AND DISCRETE APPROACHES TO THE STATICS OF MASONRY VAULTS

Mariella De Piano

Il Tutor
Prof. Valentino Paolo Berardi
Il Co-Tutor
Prof. Fernando Fraternali

Il Coordinatore
Prof. Fernando Fraternali

Fisciano, 5 aprile 2019

To Ugo, Marina, Aniello and Raffaella

CONTINUUM AND DISCRETE APPROACHES TO THE STATICS OF MASONRY VAULTS

Abstract

This dissertation presents continuum and discrete approaches to the statics of masonry vaults.

The thrust surface concept is introduced within Heyman's safe theorem and extends the funicular curve to the 3D case. A variational formulation of the truss network of masonry vaults is presented and allows to search a 'safe' thrust surface within a design domain. Such a model is based on a scalar potential φ of the stress carried by the thrust surface S (Airy's stress function) and polyhedral approximations to φ, by a predictor-corrector strategy based on the convex hull technique (no-tension model).

In the same way, a static load multiplier for curved structures is iteratively obtained and validated, by increasing the live loads over several steps and verifying, for each interaction, the existence of a corresponding statically admissible state of equilibrium via lumped stress method. Using this approach, we can observe potential cracks, where the stress state is unidirectional.

A tensegrity model of reinforced vaults is also proposed and allows to perform a design minimal mass reinforcements of masonry vaults under static and seismic loads.

Several case studies of unreinforced and reinforced masonry vaults are presented and discussed.

.Acknowledgments

The author wishes to thank:

Fernando Fraternali, Valentino Paolo Berardi, Ada Amendola, Gerardo Carpentieri, Raffale Miranda, Ida Mascolo, Giuseppe Rocchetta, Luciano Feo, Geminiano Mancusi, Rosa Penna, Marco Lamberti, Agostina Orefice, Maurizio Angelillo, Antonio Fortunato, Francesco Ascione,

research group of Structural Mechanics of Department of Civil Engineer (DICIV) of University of Salerno

for their precious advices, collaboration, support, solidarity and friendship during the course of my PhD.

The author also wishes to thank:

Gianmario Benzoni for the precious and unique teaching on the study of seismic isolators at *Department of Structural Engineering and Caltrans Testing Facility, University of California, San Diego, USA* (March – June, 2018)

and

Anthony Rosato for the immense hospitality and opportunity of collaboration with his research group on the study of software Impetus-AFEA at *Granular Science Laboratory, New Jersey Institute of Technology, USA* (July-August 2019)

Publications

The work presented in this dissertation originated the following articles published in international scientific journals and conference proceedings:

Berardi V.P., **De Piano M.**, "On the statics of curved masonry structures via numerical models", PSU RESEARCH REVIEW, 1-8, 2018. ISSN:2399-1747, DOI: 10.1108/prr-07-2018-0020.

Rocchetta G., **De Piano M.,** Berardi V.P., Fraternali F., "On the shape optimization of the force networks of masonry structures", International Journal of Masonry Research Innovation, 4 (1/2), 78-96, 2018. ISSN: 2056-9459.

Berardi V.P., Feo L., Mancusi G., **De Piano M.,** "Influence of reinforcement viscous properties on reliability of existing structures strengthened with externally bonded composites", *Composite Structures* 200, 532-539, 2018. ISSN:0263-8223, DOI: 10.1016/j.compstruct.2018.05.111.

De Piano M., Modano M., Benzoni G., Berardi V.P., Fraternali F., "A numerical approach to the mechanical modeling of masonry vaults under seismic loading", *Ingegneria Sismica/International Journal of Earthquake Engineering* 3**4**, 103-119, 2017. ISSN:0393-1420.

Berardi V.P., **De Piano M.,** Teodosio G., Penna R., Feo L. "Adaptive models of no-tension masonry vaults", AIMETA 2017, Proceedings of the XXIII Conference, The Italian Association of Theoretical and Applied Mechanics, Mediglia (MI) GECHI EDIZIONI by Centro Servizi d'Ateneo S.r.l. 3,1402-1414, 2017. ISBN:978-889-42484-7-0.

Berardi V.P., Chiozzi A., Fraternali F., Grillanda N., **De Piano M.,** Milani G., Tralli A. "A numerical approach to the evaluation of collapse load multiplier of masonry curved structures", AIMETA 2017, Proceedings of the XXIII Conference, The Italian Association of Theoretical and Applied Mechanics, Mediglia (MI) GECHI EDIZIONI by Centro Servizi d'Ateneo S.r.l. 3,1515-1525, 2017. ISBN:978-889-42484-7-0.

Berardi V.P., **De Piano M.,** Teodosio G., Penna R., Feo L. "Advanced numerical models for the analysis of unreinforced and strengthened masonry vaults", COMPDYN 2017, 6th ECCOMAS Thematic Conference on Computational Methods in Structural Dynamics and Earthquake Engineering

Athenes Institute of Structural Analysis and Antiseismic Research School of Civil Engineering National Technical University of Athens (NTUA) 2,5056-5069, 2017. ISBN:978-618-82844-3-2.

Berardi V.P., **De Piano M.,** Teodosio G., Fraternali F. "Evolutionary strategies for the FRP/FRCM-reinforcement of masonry vaults", In: ICCS19 Conference Proceedings 19° International Conference on Composite Structures, Bologna Esculapio 1, 65, 2016.

Carpentieri G., Fabbrocino F., **De Piano M.,** Berardi V.P., Feo L., Fraternali F. "Minimal mass design of strengthening techniques for planar and curved masonry structures", In: Proceedings of ECCOMAS Congress 2016 Crete Island ECCOMAS 4654,1-10, 2016. DOI: 10.7712/100016.1954.4654

Berardi V.P; **De Piano M**., Teodosio G., Bilotti G; Fraternali, F. "Innovative modeling of unreinforced and FRP/FRCM strengthened vaults", In: International Workshop "Multiscale Innovative Materials and Structures" (MIMS2016) 2016, Pag.1-1, (DOI): 10.13140/RG.2.2.21778.86728.

Farina, I., Fabbrocino, F., **De Piano M**., Feo, L., Fraternali, F."Use of 3D printing techniques to improve the mechanical response of cementitious composites", In: 2nd International Conference on Mechanics of Composites, Bologna Esculapio 1, 50, 2016. ISSN 2421-2822, ISBN 978-88-7488-963-1, DOI 10.15651/978-88-748-8963-1.

During the course of my PhD studies, I have also acted as co-author of the following journal articles and conference proceedings, which are concerned with different topics:

R. Singh, N. Singh, I. Farina, I. Mascolo, **De Piano M.**, A. Amendola , F. Fraternali "Green design of novel metal matrix composites", February 2019 IOP Conference Series Materials Science and Engineering 473(1):012008, DOI: 10.1088/1757-899X/473/1/012008.

R. Singh, N. Ranjan, I. Farina, **De Piano M.**, A. Amendola, F. Fraternali "Mathematical modeling of surface roughness in the forming of innovative materials", February 2019 IOP Conference Series Materials Science and Engineering 473(1):012009, DOI: 10.1088/1757-899X/473/1/012009.

R. Singh, N. Ranjan, I. Farina, **De Piano M.**, A. Amendola, F. Fraternali "Mechanical and experimental study on the use of sustainable materials for additive manufacturing", International Conference on Advanced Materials, Mechanics and Structural Engineering, February 2019 IOP Conference Series Materials Science and Engineering 473(1):012010, DOI:10.1088/1757-899X/473/1/012010.

R. Singh, N. Ranjan, I. Farina, **De Piano M.**, A. Amendola, L. Feo, F. Fraternali "Innovative sensing elements based on graphene" International Conference on Advanced Materials, Mechanics and Structural Engineering, 2018, Seoul, Korea (*in press*).

Amendola A., Krushynska A., **De Piano M**., Daraio C., Pugno N.M., Fraterrnali F. "Mechanical modeling of the bandgap response of tensegrity metamaterials", ICNAAM 2018, 16th International Conference of Numerical Analysis and Applied Mathematics, 2018, Rhodes (*in press*).

Mascolo I., Amendola A., **De Piano M**., Feo L., Fraternali F. "On the equilibrium problem and infinitesimal mechanisms of class theta tensegrity systems", ICNAAM 2018, 16th International Conference of Numerical Analysis and Applied Mathematics, 2018, Rhodes (*in press*).

Contents

LIST OF FIGURES

LIST OF TABLES

Part I. Introduction

The masonry is one of the oldest building materials. It can be defined as a composite material, not homogeneous, made up of interlocked or not worked blocks between them, dry or through bedding mortar. The nature of blocks is varied (natural stone, brick, adobe) in the historical heritage. The variability depends on the local factors such as traditional construction methods related to the geographical area, to the culture of the population, from the availability of the type of constituent elements.

Figure 1: Masonry bridge "Pietra dell'Oglio", 2nd century BC until, Monte Verde (AV).

Romans only began to achieve significant originality in architecture around the Imperial period (Figure 1), using different assembly techniques of this material and creating structures still existing and in good health.

Giuffrè [1] underlines two kinds of masonry techniques, the popular and the educated one. The first is built by the inhabitants themselves builders and it represented by vernacular architecture. It is very common built in the territory. On the other hand, the second one is built by professional workers according to strict geometric rules build the second.

Vitruvius [2] considers to the Greek builders the creators of the “opus quadratum”, characterized by the use of machined and squared stone elements. The blocks, organized on horizontal rows with vertical joints, are positioned respecting to the “isodoma” or “pseudo-isodoma” order, in rows of the same height and of variable height, respectively. A connection between blocks is created by the two types assembled masonry. They give to the masonry a monolithism obtained by the assembly of the constituent elements, i.e. diatonos and orthostats (Figure 2).

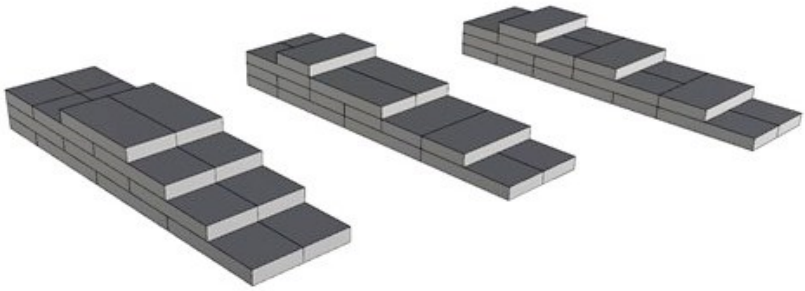

a) b) c)

Figure 2: Masonry walls: (a) wall with orthostats; (b) wall with diatonos;(c) wall with the alternation of orthostats and diatonos on the same row.

Although masonry structures have lasted for hundreds of years and being one of the earliest types of structures undergo scientific structural analysis, they are often considered difficult to analyze or to assess in a precise way. This approach is partially due to the usual uncertainties in assessing built structures: the presence of unknown or uncertain material properties, the difficulty of obtaining correct measurements, and the difficulty of evaluating the conditions of these structures without the possibility to control the interior of the structure.

Based on these considerations, the purpose of this thesis is to offer useful approaches to the analysis, conservation and restoration of these structures with a particular focus on vaults.

1.1 State of the art

Among the structural elements in masonry buildings, arches and vaults are very widespread in European historical centers. Their preservation represents the preservation of the cultural heritage, as well as the architectural one. A lot of

attention has been paid to the accurate design and stability of masonry arches and vaults.

Particularly, under a geometrical point of view (Figure 3), the study of these characteristics was already felt from the Roman to the Renaissance age, but the presence of horizontal thrusts was already perceived in the 1st–century B.C. [3].

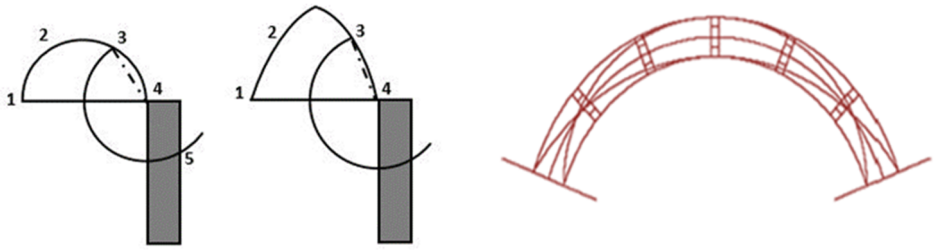

a) b)

Figure 3: (a) Geometrical design rule still used during 18th-century; (b) Configuration of the thrust line by Barlow (1846).

Main developments and reviews in the study of historical masonry arches and vaults can be summarized as follows:

- Robert Hooke [4] and David Gregory [5]. The mathematical formulation of the catenary curve. They employed the analogy between a hanging chain and an arch, the latter introducing the simile of a necklace made by smooth spheres that, overturned, could stand up by blocking the ends.
- Giovanni Poleni [6] applied this formulation to examine the dome of Saint Peter's Basilica in Rome.
- Philippe de la Hire [7]. The concept of collapse. A collapse mechanism is identified through a division of an arch into three rigid blocks, moving without friction.
- Claude Couplet [8] analyzed the concept of collapse mechanism due to mutual rotations between adjacent portions, considering qualitatively the friction effects.
- Charles Coulomb [9]. The equilibrium approach. Four possibile collapse mechanisms are identified, considering in each case a limit load that could guarantee the equilibrium condition of the arch.
- Louis-Claude Boistard [10] tested numerous 5-meter scaled models, establishing the four-hinge mechanism collapse of an arch.
- František Josef Gerstner [3]. The thrust line. A thrust line of a vault is defined as a function of shape and load.

- Louis Navier [3] applied the theory of elasticity to the arch, including in the analysis the strength of materials.
- Henry Moseley [11] defined the thrust line as tangent to the intrados at the haunches and tangent to the extrados at the middle section, in the condition of the minimum horizontal force.
- Eugene Mery [3] considered instead, a different condition of the thrust line, by means as contained in the central third of each section.
- Heyman [10][12]. The limit analysis based on the Heyman's hypothesis. The collapse of a masonry arch occurs when a certain number of potential hinges is created. This condition occurs in the case of the thrust line is not contained in the extrados and intrados of the arch in a number of points sufficient to produce the condition of lability (Figure 4).

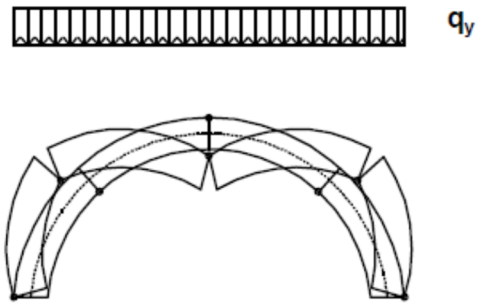

Figure 4: Collapse mechanism formed by the creation of plastic hinges.

Based on these considerations, the so-called modern vault theory by Heyman consists of a limit analysis approach to the statics of masonry arches and vaults based on the following assumptions:

- masonry has no tensile strength;
- masonry has infinite compressive strength;
- sliding between masonry parts does not occur (no-tension model).

The first condition occurs since the mortar, which links the joints, could be deteriorated. The second assumption is the consequence of the first, due to the fact that the compressive rift is not likely to succeed, because the tensile stresses are lower than the compressive strength. The last hypothesis is justified because frictions in the joints avoid the sliding of the stones.

The equilibrium condition is satisfied when it is possible to draw infinite thrust lines contained in the thickness of an arch. The maximum and the minimum value of the thrust line indicates the limit conditions. If the arch thickness is incrementally reduced, the limit values of the thrust line reach the value of the thickness. This condition produce the incipient collapse of

the structures. The ratio between the actual thickness and the limit value can be considered the geometrical factor of safety.

- Focacci [14] defines a limit analysis of a semicircular arch with fixed supports and shows that a masonry arch needs the formations of four hinges to produce a kinematic mechanism (Figure 5).

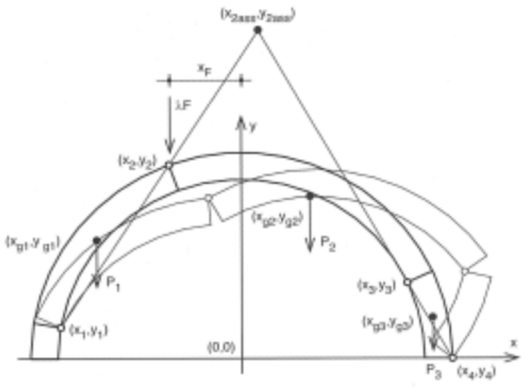

Figure 5: Scheme of limit analysis of an arch with fixed support by Focacci [122].

These examples testify the growing interest in this study. The preservation and repair of historic masonry structures has created a need for accurate and efficient analysis. Over the time, different models have been implemented to reconstruct the behavior of these structures. The behavior of masonry depends on the assembly, construction modalities of the elements and not only on the mechanical properties of stones and mortars. A research focus of fundamental interest is to provide reliable forecasts about the behaviour of these structures [15].

The masonry structures represents an aggregate of two basic components: the blocks, in stone or brick, and the mortar.

The generic composite element of this structure can be analyzed by two different methods: homogenization techniques, having a homogeneous model equivalent to the real material, or a heterogeneous model, which use different mechanical behaviours or mechanical parameters for the two components and adequate boundary conditions. In the first case, the homogenization give the possibility to describe the macroscopic behavior of the volume element through anisotropic constitutive bonds.

In many situations of technical interest (masonry with regular "weaving"), an orthotropic macroscopic bond is sufficient for practical purposes.

Some of the most relevant constitutive models available in the literature are presented for the masonries, both homogeneous and heterogeneous.

1.1.1 Heterogeneous – Discrete models

A masonry structure can be analyzed by discretizing the mortar blocks and joints separately. In this case, for each phase an appropriate constitutive law is introduced, which must also consider the interaction of each individual component with the whole of the masonry structure.

Two distinct approaches can be followed in the finite element modeling: in the first, the joints between the blocks are discretized using finite elements of appropriate dimensions, while, in the second, the "joints" elements are replaced by particular contact constraints between the blocks (boundary conditions).

The first approach requires a considerable computational burden for the analysis of real structures and in fact is almost exclusively used for the analysis of the stress state of small masonry elements.

In the second approach, however, the use of interface laws allows to use only "brick" elements, equipped with appropriate constitutive laws.

Obviously, each block must always be modeled using at least one finite element. Therefore, the dimensions of the numerical problem grow very rapidly with the increase of the complexity of the structure in all heterogeneous models.

- Page [17]. The masonry is discretized in blocks with elastic-linear and isotropic behavior linked by "linkage elements" (or "links") of punctual type. The "links" have a fragile tensile behavior and a bilinear elastoplastic behavior in compression. This model can be used for walls subject to shearing but is not able to describe, for example, collapse due to crushing.

- Lourenço et al. [18][19]. Model with interface laws derived from the Mohr-Coulomb criterion. Admissible compressive and tensile stresses in the blocks are described by introducing two suitable limit surfaces: the closing surface and the “cut-off" surface. Both the Mohr criterion and the "cut-off" surface vary according to a hardening law, while the closing surface does not evolve with the deformation state. Sliding and opening mechanisms are located inside mortar joints, while the compression collapse involves the whole masonry structure.

- Lofti and Shing [20]. Model with interface law characterized by a hyperbolic elastic limit function (generalization of the Mohr-Coulomb criterion). Unlike the model of Lourenço, Lofti and Shing use the yield surface of the interface bond, which has a

continuous gradient at each point. The limit compression of the blocks is governed by the Von Mises criterion, while the tensile failure is described by the Rankine "cut-off" surface. The Lofti and Shing model can simulate both the creep and the compression compaction of the joints, through a non-associated plastic flow law. The elastic limit function of the interface evolves according to a "softening" model.

- Gambarotta and Lagomarsino [21]. The behavior of the mortar is modeled using methods of damage mechanics. The damage to the joints is measured by an internal variable associated to a rate of release of the deformation energy, which includes inelastic terms of sliding and dilatation. Blocks damage evolves when the rate of energy equals the specific fracture energy (or toughness) of the joints, that depends in turn on the damage variable.

1.1.2 Homogeneous – Continuum models

The homogeneous models are based on the introduction of a homogeneous equivalent continuous element to represent the composite masonry. The characteristics of this element can be defined by introducing an appropriate constitutive bond capable of representing the macroscopic behavior of the masonry, starting from the mechanical properties of the components (blocks and mortar), through homogenization techniques (Figure 6).

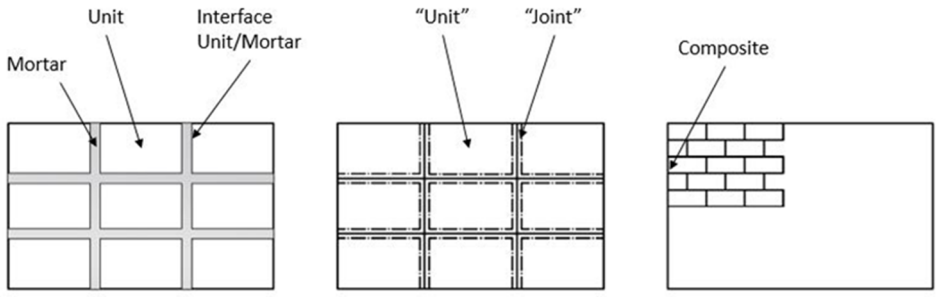

Figure 6: Modelling strategies for masonry structures: a) detailed micro-modelling; b) simplified micro-modelling; c) macro-modelling [19].

- No tensile rigid or elastic model. This is the first constitutive model formulated for the masonry, used since ancient times, for the design and the verification of these structures.

This approach is used in arches and vaults for the graphic construction of the funicular polygon [22] of a plane system of forces and in the limit analysis of plain or spatial masonry structures.

One of its first application in the rigid no-tension model, can be found in the famous work by J. Heyman "The Stone Skeleton" (1966) [12], which presents several examples of limit analysis of masonry structures of different types. A. Signorini (1925), who considers it as a prototype of a unilateral constitutive law, can trace the first mathematical arrangement of this model back to some pioneering studies.

The study of its mathematical properties has been the object of attention by numerous authors, coming mainly from the Italian school [23][30].

This model is a simple model, in which provides the material reacts rigidly or elastically in compression and is not able to withstand any tensile stress. It is able to describe with a continuous theory the phenomena of cracking typical of the masonry structures. Effects of friction between the blocks are ignored. The rigid model reproduces the behavior of historical or degraded masonry, in which the mortar is equipped with reduced tensile and shear properties.

Main characteristics of this model are described as follow.

Ganju [31]; Chen [32]; Shing [33]. Isotropic macro-models derived from experimental results, based on generalizations of the constitutive models commonly adopted for cement conglomerate. These models are useful for reinforced masonry with concrete inclusions, which do not take into account the mechanical anisotropy of ordinary masonry, due to the presence of mortar.

- Samarashinghe and Hendry [34][35].Elasto-fragile anisotropic macroscopic models respect to a limit domain of the stresses in the field of tension-compression coupled stresses (a limit resistance for pure compression is not introduced). Local stiffness and resistance are set to zero, when the stress state reaches the limit surface.

- Page et al. [36]. Anisotropic elasto-fragile model in the field of coupled tension-compression stresses and elasto-plastic model in the field of pure compressive stresses. By introducing this model into a finite element code, the two non-linearities plasticity and breakage, are treated separately. One is constant while the other evolves. The limit surface of the material refers to the plane of the voltage components relative to the directions of the joints. Each component of the plastic deformation is linked only to the homonymous stress component, through a polynomial law.

- Contro and Sacchi [37]. Generalization of the Page model with the introduction of a zero tensile strength and a plasticity with a plastic hardening compression behavior. A limit domain is enclosed by six flat faces in the field of biaxial compression stresses, considering different orientations of the principal efforts with respect to the joints.

- Pietruszczak and Niu [38]. Continuous model obtained through a double homogenization procedure, to take into account the stratifications both horizontally (mortar) and vertically (butt joints). Mortar is treated as elementes of material weakness, while butt joints are treated as inclusions characterized by lower mechanical properties compared to blocks. The collapse of homogenised material can occur both by crushing the blocks and by opening and / or sliding the horizontal joints. In the first case, an elasto-fragile behavior of the butt-joint-block system is introduced, while in the second case the collapse is described by an elastic-plastic behavior. This anisotropic model is particularly suitable for the study of masonry collapse under biaxial stress conditions.

- Papa and Nappi [39]. Unilateral evolutionary damage models with three internal variables that separately describe the damage produced by tensile stresses, compressive stresses and shear stresses. The damage model applied to each component of the mansory is a fragile type and is capable of reproducing the recovery of stiffness that is observed experimentally when compressive stresses overlap with pre-existing tensile stresses ("unilateral effect"). This approach is also capable of describing shear damage effects of the same order of magnitude as damage effects due to normal stresses. The stiffness matrix of the composite material is obtained by numerical homogenization techniques (of the representative volume element type), starting from the damage models of the base materials.

- Gambarotta and Lagomarsino [40]. Continuous pattern obtained by homogenization of a stratified medium. Laws for damaging of the blocks and mortar are described according to two suitable internal variables. One describes the damage to the mortar, while the other describes the damage by crushing the blocks. The evolution of damage is explained by considering the solution of a linear complementarity problem. This model allows to evaluate the energy dissipated by the material under cyclic loads, which represents a very important parameter for the evaluation of the seismic vulnerability of masonry buildings.

- Luciano and Sacco [41]. Damage model obtained by homogenization techniques of the "unit cell" type. The recurring element (cell) is made up of an entire block, four portions of adjacent blocks (of a quarter size of an entire block), two whole joints horizontally and vertically and two vertical half-joints. The law of damage

provides that the fractures can develop only along the horizontal and vertical joints, characterized by an elastic fragile constitutive law and the blocks are instead indefinitely elastic elements. It is admitted that the thickness of the joints is very small and that the collapse of a joint, is total. Eight distinct damage states of the unit cell are defined, each corresponding to a different "crack pattern" in the joints. It is admitted, in particular, that a joint affected by collapse can no longer be restored. The homogenization theory is used to determine, numerically, the elastic modules of the intact and cracked masonry. A model of damage evolution is also proposed. This is a very valid modeling for ancient or degraded walls, in which the tensile strength of the mortar is much lower than the resistance (tensile and compressive) of the blocks and therefore the fractures develop mainly along the joints.

- Callerio and Papa [42]. Evolutionary elastoplastic damage models for the simulation of wall behavior under cyclic loads. The masonry is described as a continuous orthotropic in a flat state of tension. Its behavior is elastic until the stress state is internal to an elastic domain limited by eight flat surfaces in the space of the Cartesian stress components (referred to the directions of the joints). The limit surface provides a reduced resistance of the material to the states of pure traction and traction-compression. When the state of tension reaches the border of the elastic domain, inelastic deformations are activated on the basis of an associated plastic flow law. At the end of each "step" in which the load law is subdivided, incremental inelastic deformations are decomposed into a properly plastic part and into a part of damage, to which a reduction of the elastic stiffness of the material is associated.

- Luciano and Sacco [43]. Damage models for walls reinforced with composite materials ("Fiber Reinforced Plastics" or FRP) obtained by homogenization techniques.

- Milani and Tralli [44]. Micromechanical model for unreinforced walls able to treat both the elastic behavior of the base materials (bricks and mortar) and the case of elastic-plastic behavior. The homogenization technique adopted is based on an approach to tensions, which uses appropriate generalizations of the principle of minimum complementary energy. The model corresponds well to the experimental results of Page (1981) and manageable from the numerical point of view.

1.1.3 Masonry vaults

The vaulted masonry structures are presented as constructive elements of absolute specificity and with characteristics that differentiate them from other recurring types used in the past to adapt to environments.

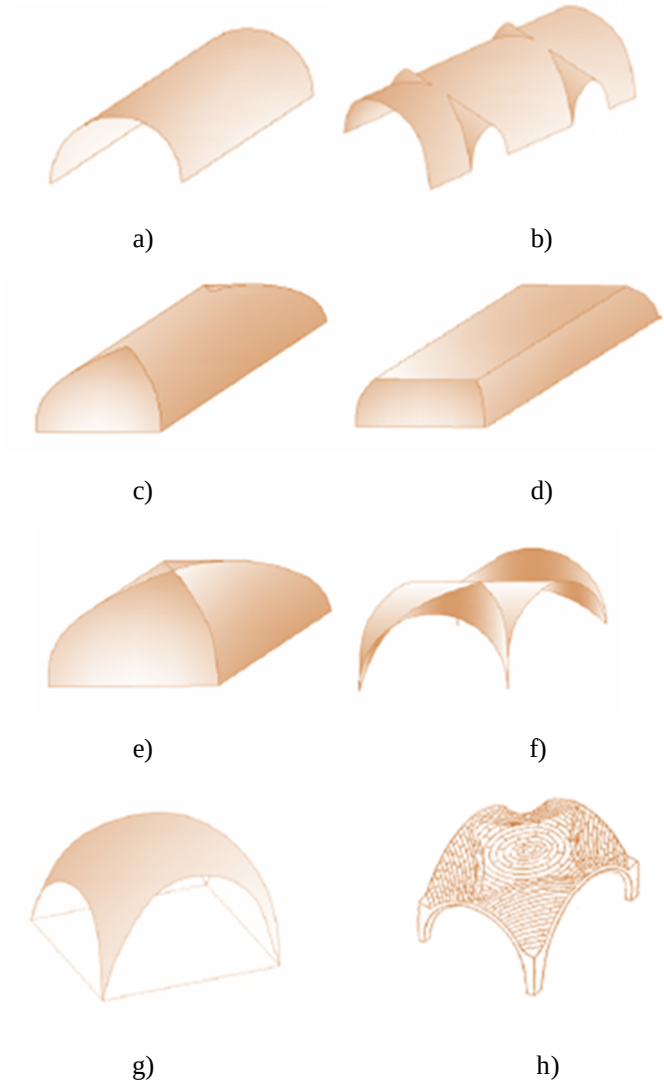

Figure 7: Main types of simple and complex vaults: a) barrel vault; b) barrel vault with lunettes; c) trough vault; d) mirror vault; e) cloister vault; f) groin vault; g) ribbed vault; h) fan vault [48] .

In general, the vault is defined as a curved surface having resistance characteristics, whose bearing capacity and structural efficiency depends on its conformation. A vault is geometrically generated by the translation (or rotation) of a curve (or of a line), said directrix, with respect to a line (or a curve) called generatrix.

Many classifications about the shape of these structures are available in various literature. Vaults are classified mainly into two groups: simple vaults (like barrel,

sail and cup vaults), derived from a single translation of the generatrix on directrix and composed vaults (like groin, cloister) defined by the composition of simple vaults. Figure 7 shows main examples of vaults.

Many of these structures may be found in the architecture of historic buildings and have had an evolution in complex geometries and shape, over the years. In particular, many examples of unusual vaults are present in Western architectural tradition.

Figure 8: King's College Chapel [124].

Figure 8 shows King's College Chapel. The fan shapes are created as a result of piers rising up in expanding cone-like shapes with elaborate ornamentation. The visual complexity is more a function of the sculptural treatment than the sternotomy. It's one of the great last great triumphs of Gothic.

Examples of recent vaults and domes are instead attributed to Antoni Gaudi (Figure 9), Heinz Isler and many other architects, who take care not only of the form but also of a targeted research of new materials more suitable to make these structures innovative.

Some aspects of the structural behavior of masonry vaults have not yet been sufficiently investigated by scientific literature and, given their complexity, can hardly be solved through classic schemes and models.

Figure 9: Crypt of the chapel of the Colonia Guell [125].

The present work aims to fill these gaps and to study in-depth some important aspects concerning the structural analysis of vaults.

Masonry vaults are often schematized as a series of non-interacting side-by-side arches. This schematization, acceptable for simple vaults, deviates from reality in the case of complex vaults, in which, due to their particular geometric conformation, can create non-negligible three-dimensional effects.

Despite the variety of examples of vaulted structures, a more detailed description will be applied to complex vaults. In particular the groin and pavilion vault are described in this part. The numerical examples, proposed in this thesis, will be mainly applied to this kind of vaults.

1.1.3.1 Groin vault

Numerous studies [45][46] have investigated the structural role of cross vaults, through the analysis of exemplary cases. However, these studies showed the enormous difficulties linked to the evaluation of the effectiveness of the structural elements that constitute the vaults in the medieval period, which vary according to the historical period, the characteristics of the materials and the construction techniques used.

What is certain is that the cross vault, rationally composed of ogive supporting arches, which intersect diagonally, and by perimeter arches, two transverse to the nave and two perpendicular, distribute the weight not on the entire perimeter wall, but on determinate points of the supports and due to this it was possible to replace the walls with windows or thin dividers.

Figure 10: Groin vaults of the Valencia Cathedral.

Romans developed the groin vault, some achieving significant widths although the barrel vault had been more widely used in earlier civilizations. King Attalos I of Pergamon constructed the first groin vault in Europe in about 223 BC in Delphi. Church architecture in the Middle Ages, was influenced by the application of groin vaults to vast halls. Figure 10 shows groin vaults of the Valencia Cathedral, dedicated to the Assumption of Mary (13th century). The groin vault was widely used for its ability to create strength, without massive buttress formations; in addition, it gave the church architects a solution for the dim light inherent in the

barrel vault design, because the barrel vault could not contain windows because it had to be strong.

The Gothic architects attempted to counteract the thrusts with counter-thrusters (like the flying buttresses) or by verticalizing the thrust by means of vertical weights (pinnacles), therefore they created a dynamic connection, which, although in a much more obvious way, takes up the system of thrusts and counter-thrust which the Byzantines had already used.

Medieval architects developed the static system, based essentially on the concept of ensuring the main aisles were as stable the principal nave, while Gothic cathedrals used ribbed cross vaults with pointed arches to empty the masonry.

From the end of the eleventh century, the diagonal arches were used in the construction of cross vaults because they were simpler to build and more stable as the transverse and diagonal arches become supporting structures, emphasized by ribs and members. The key of the cross vaults is released, because the bowing keys of the diagonal ribs are at a higher level than the arches and this also means that the vault is generated in this way.

Figure 11: Hauptbahnhof Station in Berlin [126].

20th-century structural engineers have adopted the static stress forces of the groin vault design and confirmed the Romans expertise in efficient design to accomplish a wide span of construction, the multiple goals of minimum materials use, ability to gain lateral illumination, and therefore avoiding lateral stresses. Europe's largest train station, Hauptbahnhof in Berlin (Figure 11), which has an entrance building with a glass-spanned groin vault design is an excellent modern example of architecture.

1.1.3.2 Cloister vault

The masonry cloister vault, although used extensively starting from the sixteenth century as a cover for most typical buildings, have never been studied in depth,

probably because of the obvious difficulties encountered in applying simplified theories to this complex type of vault.

It may be thought of as being formed by two barrel vaults that cross at right angles to each other: the area within the vault is the intersection of the space within the two barrel vaults, and the solid material around the vault is the joining together of the solid material surrounding the two barrel vaults. We can see that it differs from a groin vault - formed from two barrel vaults but in the opposite way: in a groin vault, the empty area is the union of the spaces of two barrel vaults, and the solid material is the intersection.

The pavilion vault, like all type of vaults, exerts thrusts to the support that often, especially in the case of large vaults, are too high and result in the removal of the perimeter walls. In addition to this type of problem, they often present significant lesions along the diagonals.

Scientific literature, up to now, has not been able to produce valid models that permit the simulation of the structural behavior of pavilion vaults. This is due to a lack of knowledge of the complex static mechanisms that are generated within them and the lack of a theory able to grasp the real state of stress before and after cracking.

Cloister vaults, in fact, in spite of their widespread use, have not been an area of study in scientific literature. Although, there have been interesting contributions in some studies [47][48].

Seeing the importance of studies regarding the pavilion vault and their application and use, this work concentrates on the methods of calculation on the discrete and continuum approaches on the statics of this vault. From this, we can easily find the applicable calculations required for the principle static mechanism of the pavilion vault, leading to eventual consolidation.

The Romans used pavilion vaults as early as the 1st century B.C.

The Tabularium (78 B.C.) and the temple of Hercules in Tivoli (80-85 B.C.) contain the first examples. Further vaults may be seen in the Domus Aurea (64-68 A.D.), in the Domus Augustana (81-92 AD), in the Villa Adriana in Tivoli (117 A.D.), in the baths of Antoninus in Carthage (145-160 A.D.) and in those of Diocletian (298-306 A.D).

Cloister vaults, widely used for the covering of polygonal rooms, continued to be used in chapels of religious buildings and in baptisteries.

The intersection between the transept and the central nave, once a pavilion on an octagonal plan, became widely spread. We can find such examples in the Church of

Sant'Ambrogio in Milan (Figure 12) and in that of San Michele Maggiore in Pavia (Figure 13).

Cloister vaults and all its variations began to be used in residential architecture from the 16th century onwards, to cover the halls of the palaces, mainly due to their ability to completely transfer the load onto the surrounding walls.

Palladio was the first to illustrate, through a very concise description and a series of figures, the six ways to construct vaults, the type of which was chosen depending on the room that was to be covered. He proposes the barrel vaults with heads of pavilion, called a basin, should have the arrow equal to one third of the width of the room.

Later, Scamozzi proposed his designs for the six types of vaults, but furthermore he proposed an innovation, which was the concept of a pavilion vault to cover a room. He also realized that the cloister vault is easier to realize thanks to its geometric configuration.

Guarino Guarini subsequently, proposed that pavilion vaults are realized starting from a half-cylinder cut diagonally. Guarini also said that the plinth on which pavilion vaults rest can be of a variety of forms from square to octagonal.

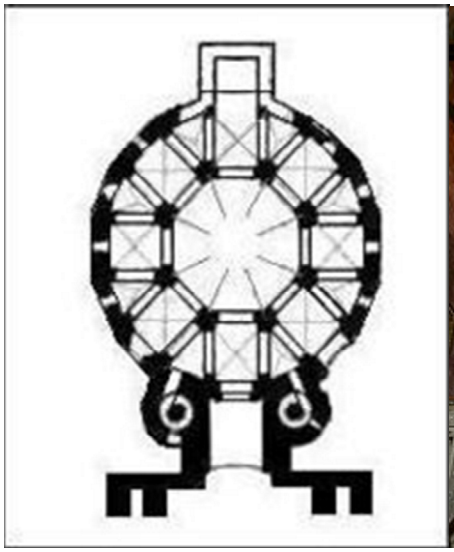

Figure 12: Plan of the Palatine Chapel of Aachen [127].

Figure 13: The cloister vault in the Basilica of S.Michele Maggiore [128] .

Architectural manuals began to report real practical information on the geometry and construction of the pavilion vault and its main types, starting from the nineteenth century. The pavilion vault is set on a square plan and is created by the union of four

cylindrical spindles that make up the intrados surface (Figure 14), so Alberto Castigliano defined the cloister vault in the practical manual of Engineers.

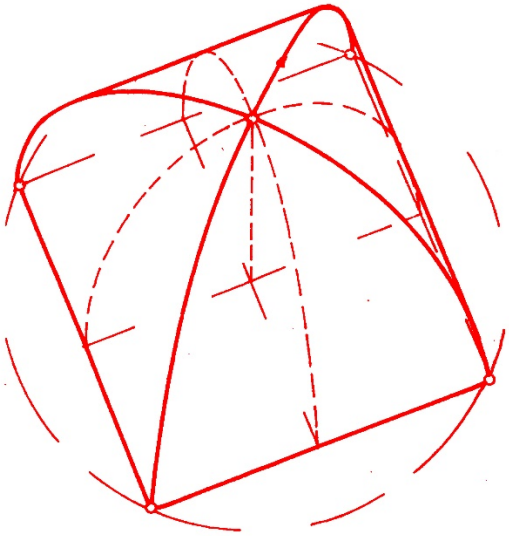

Figure 14: Design of cloister vault by Alberto Castigliano [129].

1.2 Problem statement

The funicular curve method dealing with masonry arches has been applied to 3D problems over recent years, by using either continuous or discontinuous approaches. Continuous approaches typically are based on stress-function formulations of the equilibrium problem [49][51] or maximum modulus eccentricities surfaces [52][53], while discontinuous approaches describe the no-tension stress field through spatial force networks generated via 3D funicular constructions [54][56].

The present study deals with different approaches to the statics of masonry vaults by researching a ‘safe’ thrust surface in different load conditions.

In particular, we focus on discrete approaches to find the optimal thrust surface and the corresponding state of stress.

Starting from the formulation in terms of the function of Airy stresses of the boundary value problem, an approximation has been proposed with polyhedral test functions (piecewise linear) on a triangulation called primary mesh.

This approximation, of a non-conforming type, generates concentrated tensions along the interfaces of the primary mesh (Concentrated Tension Method or "Lumped Stress Method"), which can be considered as the axial stresses borne by the rods of

a reticular structure [57][58].

The discrete problem depends on the nodal values of the Airy function and is solved by minimizing an appropriate functional energy that depends on both the shape of the surface and the stress state, expressed through the aforementioned function.

From the physical point of view, the functional represents the complementary energy of the reticular structure that approximates the continuous medium. It is an unconventional type of energy, which couples the contributions of the convergent stress in the same node.

The method is particularly effective in the case of problems characterized by singularities of the stress field (concentrated forces, edge effects, cracks, transition from 1D elements to 2D elements, etc.). Moreover, it can easily be generalized in flat problems with constraints on the state of tension (holonomic plasticity, non-tensile strength, etc.).

In previous works, the convergence of the method in the case of planes of loading problems has been mathematically proved, using typical arguments of the mixed methods to the finite elements. In particular, its convergence speed has been demonstrated, under appropriate assumptions of regularity and uniformity of the primary and secondary meshes.

Furthermore, its numerical implementation was demonstrated, with reference to the more general case of flat problems with mixed type boundary conditions; several numerical results were obtained and comparisons were established with solutions in closed form and numerical solutions to finite elements. The results confirmed the theoretical predictions and highlighted the computational agility and accuracy of the "Lumped Stress Method" (LSM).

In this work we propose to apply this method to the study of masonry vaults, taking into account the peculiarities they present, which differ from any plane problems due to the three-dimensional nature of the vaults. It is subject to internal tension that allow the structure to remain in equilibrium if subjected to actions of compression, and due to the nature of the load, which does not belong to a plane.

The theory with regard to this problem will be presented in chapter 3; we will write the equations considering a generic three-dimensional shell assuming that its behavior is membrane and then, analogous to the case of plane problems. We will refer to the surface projected on a horizontal plane, on which we will evaluate the projected tensions. Then we will pass to the variational formulation, obtaining a functional energy to be minimized that will depend both on the geometric form of the vault and on its stress state.

Within the present study several numerical simulations on vaulted structures have been developed by using this mechanical model. In particular, the case study, presented in the continuum approach, has been analyzed via LSM methodology for researching a safe thrust surface in equilibrium with applied loads. In addition, a static load multiplier is iteratively obtained, by increasing the live loads over several steps and verifying, for each interaction, the existence of a corresponding statically admissible state of equilibrium via lumped stress method.

The curvature will also be expressed as nodal values, obtained by appropriately mediating the slope jumps between the various triangles that converge in the node in question.

Such a lumped stress approach provides statically admissible force network in accordance with no-tension constraints.

Usually, relaxation methods are used to transform an ill-conditioned minimization problem into a well-conditioned one, introducing an appropriate "relaxation" of the functional to be minimized [57],[58].

The concentrated stress method, on the other hand, operates in reverse: the original function to be minimized (complementary energy of the flat body) is strictly convex on the space of the admissible functions. The introduction of a family of relaxed functionalities, dependent on the dimension h called primary and dual mesh, allows an extension of this space, introducing the possibility of modeling the stress field through concentrated stress.

In this perspective, the convergence of the method could be proved using arguments typical of the theory of convergence, that is showing that the succession of the least of the relaxed functional converges to the solution of the original problem, in a weak sense, for $h \to 0$.

As already noted, another approach was followed, demonstrating the convergence of LSM in the theory of mixed methods to finite elements.

In fact, mixed methods are often used to approximate a certain problem to partial derivatives by means of two or more sub-problems of a lower order (primary problem and secondary problem), so that the space of the admissible functions is extended.

Glowinski [118] first demonstrated the convergence of mixed methods. Subsequently, Ciarlet and Raviart [119] determined the convergence speed of these methods when interpolating polynomials of degree are used for both the primary and secondary problems, while Scholtz [120] deduced a similar result for piecewise

linear polynomials.

The peculiar aspect of the stress and concentrated deformation methods lies in the approximation used for the constraint that links the primary and secondary sub-problems (internal constraint). It allows you to decouple these two problems, ultimately reaching a minimum two-field problem (Airy function and tension field) without constraints.

The second discrete approach follows the same schematization of the first as regards the modeling of the masonry as a lattice of rods. Where it is not possible to find a solution in the case of unreinforced masonry by LSM procedure, we can use a tensegrity approach to design a non-invasive reinforcement with a linear programming technique, which defines a cloud of points through the use of modern instruments such as laser-scanners or drones.

In fact, using the LSM procedure, when the stress state in unidirectional, we have fractures of the masonry surface, which can be repaired by the selective and non-invasive insertion of fiber-reinforced elements.

Recently a study [59] has presented a tensegrity approach to the 'minimal-mass' FRP-/FRCM reinforcement of masonry domes and vaults. This method uses tensegrity concepts to create an optimal resisting mechanism of the reinforced structure, under given loading conditions, in compliance with the 'Italian Guide for the Design and Construction of Externally Bonded FRP Systems for Strengthening Existing Structures' [60]. Such an approach permits the designer to describe the response of the reinforced structure using simplified schemes, by assuming that tensile stresses are directly taken by the FRP reinforcements, and the stress level may be determined by adopting a distribution of stresses that satisfies the equilibrium conditions but not necessarily the strain compatibility. This method regards the reinforced structure as a tensegrity network of masonry rods, working in compression while the tension elements correspond to the FRP-/FRCM-reinforcements, theoretically are acting as elastic-perfectly-plastic members. It optimizes each node of a discrete model thus connecting the structure with all the neighbors lying inside a sphere of prescribed radius, in order to define a background structure with a minimal mass. Timber or steel beams/ties can naturally replace the FRP/FRCM reinforcements. The present study generalizes the approach presented in [61][62]to the case of 2D and 3D discrete models of masonry structures with arbitrary shape. This extension permits us to explore the potential of the tensegrity modeling of reinforced masonry structures in the design of non-invasive reinforcement patterns of systems formed by masonry walls, vaults and domes. We seek to formulate a design that looks for an optimal and lightweight pattern of

reinforcing elements giving rise to a minimal load bearing mechanism of the examined structure, under given loads and yielding constraints. Thanks to the safe theorem of the limit analysis of elastoplastic bodies, this mechanism ensures that the reinforced structure is safe under the examined loading conditions, while assuming elastic-perfectly-plastic response of all members. A 3D point cloud defines the geometry of the structure to be reinforced, obtainable via in-situ laser-scanning, together with the material densities and yielding strengths of masonry and reinforcing elements.

The present thesis is aimed at deepening the fundamental understanding of continuum and discrete approaches to the static of masonry vaults, and its application to the design, modeling, restoration and preservation in engineering fields where current knowledge of such systems is only partial. Attention is focused on the modelling of these structures in no-tension constraints, under multiple loading conditions.

The structural behavior of masonry vaults are investigated. This work aims to develop computational procedures, which allows defining the 3D structural behavior of complex masonry vaults.

These models allow determining the optimal thrust surface and the corresponding state of stress for generic vaults, taking into account also the 3D interactions between arches that can develop in these structures. These effects, which are negligible for some types of vaults, such as for example the barrel vaults, instead become relevant for complex vaults, such as the pavilion vaults, in which, due to their geometry. In fact, the complex mechanisms developed in their web don't allow to reduce the vault to a series of adjacent arches, without transversal connection.

The main purpose of the present work is to precisely investigate the structural behavior of masonry curved structures focusing on groin vaults and especially on cloister vaults and on trying to provide a more exhaustive discussion on the mechanisms and actions that are generated within them.

1.3 Outline of dissertation

Part I of the thesis is dedicated to the introduction of the research activities developed during the author's PhD studies, and to illustrate the major goals of such research.

Part II provides theories about the continuum approach of masonry vaults with the definition of the thrust surface in the no-tension membrane regime. The equilibrium problem of masonry vaults takes into account the characteristics of the masonry

material: heterogeneity, good compressive strength, almost no resistance to tension, and a high friction coefficient. We begin by investigating the R-adaptive finite element techniques to explain how the accuracy and the efficiency of finite element solutions can improve results in numerical examples, regarding a case study of a cloister vault. In addition, a validation of this approach is presented.

Part III defines discrete approaches: the lumped stress method and the tensegrity modeling of reinforced vaults.

These approaches can be seen as two complementary approaches. The first evaluates the static of unreinforced masonry elements and the evaluation of concentrated forces acting under static actions mainly related to their own weight and to the uniformly distributed or concentrated load. The second approach however, proposes a possible resolution technique of the first one. In fact, the tensegrity approach, also applicable under dynamic load conditions, exploits the introduction of FRP or FRCM composite elements in the areas of the thrust surface in which uniaxial stresses are present and which could result in fractures.

Numerical examples are described in part IV. We began by investigating the shape optimization of the same cloister vault, analyzed via the R-adaptive finite element techniques, in the case of unreinforced case and using the Lumped stress Method. The proposed method allows for modelling masonry structures as no-tension elements and gives, in the case of curved masonry members, the optimized surface through a predictor-corrector procedure and the stress function describing the membrane stress. The given approach offers a useful tool for predicting the crack pattern of unreinforced masonry structures and the associated fields of stress.

An extension of this approach is shown by researching the collapse load multiplier for a masonry arch and a pavilion vault, analyzed via NURBS surfaces by previous authors. This study is appropriately validated in this thesis. Such a compressive truss network is researched in the region comprised within the intrados and the extrados of the vault via an iterative procedure.

In addition, we analyze reinforced vaults under static and seismic loads of numerical examples by the tensegrity approach. Case studies dealing with the FRP-/FRCM-reinforcement of cloister and groin vaults are considered.

We end by summarizing the major points of the present study, and suggesting future directions of research for the design and testing of physical models of masonry vaults, that can be useful for engineering applications.

Part II. Continuum Approaches

The modeling, as a continuous body, is carried out through homogenization techniques, in which there is no longer any distinction between the elements that constitute the wall texture and the mortar joints. In this case, it comes as a definition of a single finite element or unit cell, which has the task of simulating the global behavior of the "masonry" material. The homogenization of mechanical properties has been in the last decades of interest to several authors and has led to the definition of multiple procedures of homogenization, now available in literature, which follows different approaches (Figure 15).

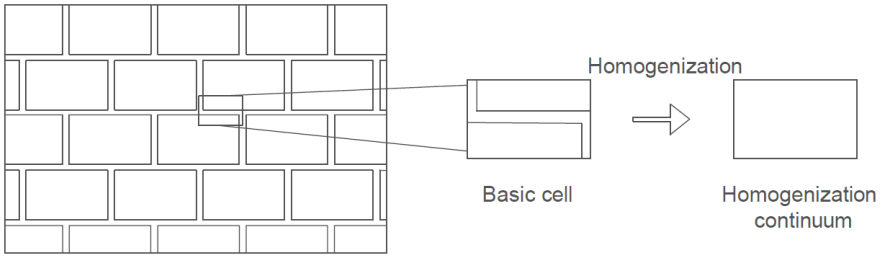

Figure 15: Procedures of homogenization

Based on this consideration, understanding the equilibrium of structures in masonry is thus of primary concern. Huerta very clearly states the importance of equilibrium methods for the analysis of masonry structures, framed in an extensive historical overview [63]. Limit analysis provides a useful guide [64][65] to determine the stability and the assessment of the safety of masonry structures. Thrust surface is defined in 3D space by using graphical methods, starting from the concept of the thrust line in 2D problems. In particular, R-adaptive finite element models are recently proposed in literature. Several numerical examples of unreinforced and reinforced vaults under different load conditions are reported in this chapter. We present the response of these curved structures by using a R-adaptive finite element model based on a Breeder Genetic Algorithm (BGA).

2.1 The Thrust Surface

In this part of my thesis, I will attempt to define a finite element approach to the search for a 'safe' thrust surface of masonry vaults or domes.
There always exists a possible equilibrium solution on any surface of thrust within the arch. The solution is not the only one. In an arch of sufficient thickness, there are infinite possible inverted catenaries or lines of thrust. The equations of equilibrium are not sufficient to obtain the inner forces, because the arch is a statically indeterminate (hyperstatic) structure.
To determinate the position of the line of thrust we can refer to many studies. The use of graphic statics is a useful method for exploring the infinite possible equilibrium solutions, may be applied to the analysis of ancient structures in unreinforced masonry and for project to construct new funicular structures. A great drawback however is the limit of two-dimensional problems. By introducing the concept of thrust surface, we can relate the geometry of the 3D-dimensional equilibrium networks to their internal forces.

2.1.1 From the thrust line to the thrust surface

Here we discuss the free-body equilibrium of an arch. A stress distribution will exist in each joint (which we imagine more or less plane) and the stresses will be compressive forces, a "thrust" and the "center of thrust" is the point of application. It will be contained within the plane of joint. Hence, the two thrusts in the joints keep the keystone even. The other stones behave in the same way until we arrive at the springing of the arch. There the abutment must resist a certain thrust. The abutment must have adequate dimensions to resist the "thrust of the arch". There are two main problems concerning masonry architecture: to design arches that will not collapse and buttresses which resist the load. Efficient use of the buttresses is fundamental because it could provoke the collapse of the whole structure.
The locus of the center of thrust forms a line, the "line of thrust." The geometry of the arch dictates the form of this line, therefore also its loads and the family of plane joints considered (the concept was first formulated by Moseley [65]and followed by a detailed mathematical treatment in Milankowitch [66].
Naturally, the line of thrust must be contained within the masonry arch to respect the main characteristics of the masonry material. It is possible to imagine one voussoir acting in tension with the other two voussoirs only via the centers of thrust. By inverting the arch, what was a force of compression becomes a tension force: the voussoirs now hang like a chain, as reported by Robison [67]. By use of the form of an inverted catenary, Hooke [4] already tried to solve the problem of the figure and

thrust of the arches (Figure 16). Hooke's affirmation: "none but the catenary is the figure of a true or legitimate arch or fornix. And when an arch of any other figure is supported, it is because in its thickness some catenary is included", was confirmed by Gregory [5] some twenty years later. Fig.18 shows the equilibrium of the arch with an inner force configuration represented by the inverted catenary by the Italian Giovanni Poleni,

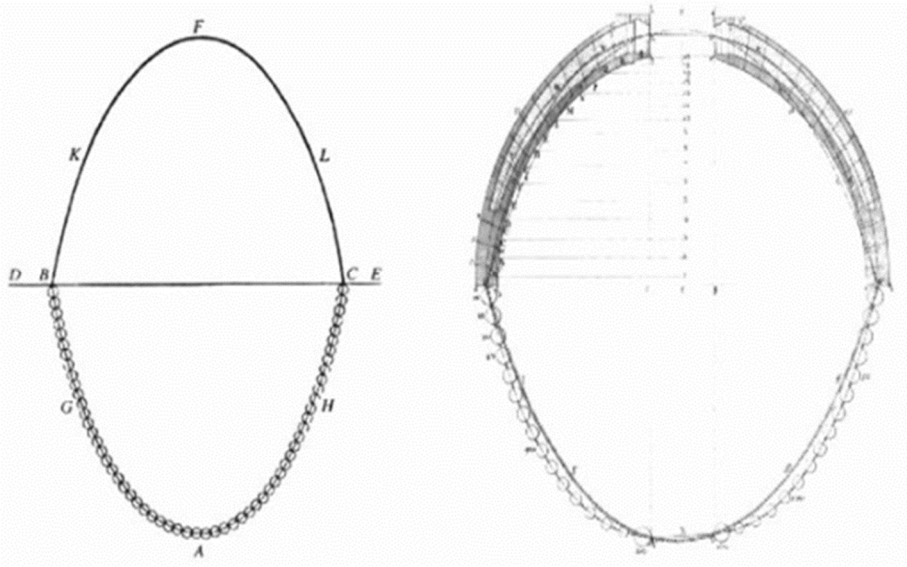

a) b)

Figure 16: a) Poleni's drawing of Hooke's analogy between an arch and a hanging chain; b) Poleni's analysis of the St. Peter's in Rome [112].

We can use thrust line analysis to explain and discuss the stability of two-dimensional (2D) structures, but it may not only be applied to them. By applying this concept to 3D surface we may define a thrust surface in equilibrium with applied loads. The force applied on a surface in a direction perpendicular or normal to the surface is also called thrust. This analysis has also been used to carry out pseudo-three-dimensional (3D) approaches [68][69], which often give rather limited results. By the use of either continuous or discontinuous approaches, many extensions of the funicular curve approach of 3D problems regarding vaults and domes have been recently suggested. The use of stress-function formulations of the equilibrium problem [49][51] or maximum modulus eccentricities surfaces are being applied to continuous approaches[52][53] while the no-tension stress field through spatial force networks generated via 3D funicular constructions [54] are described by discontinuous approaches such as the Thrust Network Analysis (TNA) [70][71] or

the Lumped Stress Method (LSM) [72][73]. When we consider continuous and discontinuous approaches based on stress-functions or the TNA, we are confined to parallel loading [52] while maximum modulus eccentricities surfaces call for fixed finite element models under certain boundary criteria [53]. In this section, the thrust surface is modelled by the R-adaptive finite element model with use of stress-function formulations of the equilibrium problem to minimize the tensile stresses.

2.2 Equilibrium problem of masonry vaults

The main cause of collapse of ancient masonry structures is foundation settlements, earthquakes, or long-term deformations [74] and not a lack of compressive strength. An optimal structural shape is vital for the equilibrium and stability of structures in unreinforced masonry.

For structures to stand with negligible tensile stresses, the implementation of an automated three-dimensional type of graphical equilibrium analysis provides a critical review of the various analytical methods for masonry arches and vaults.

The use of an equilibrium approach for ancient masonry structures is emphasized by Huerta [75][76], who also advises the application of compressive thrust line analysis to evaluate the range of probable equilibrium conditions within the wider scope of limit analysis.

This section is constrained to equilibrium analysis to masonry vaults. An important review of equilibrium methods for the analysis of masonry structures was produced by Kurrer [77].

The analysis of complex vaults with reference to the arch theory is permitted by the equilibrium approach. We may imagine the vault divided in a series of arches which permits us to look for a line of thrust inside every arch each. By achieving this, we find a possible equilibrium solution in compression and according to the “Safe Theorem”, the structure is sound.

Poncelet’s theory [78] suggested applying the elastic theory to masonry arches in order to obtain a unique solution (the theory for circular arches made of wood or iron was developed by Bresse, [79]). In spite of this, engineers were reluctant to include masonry (as we have seen, essentially heterogeneous, anisotropic, irregular) with an elastic material (uniform, isotropic, etc.). In fact, until ca. 1880, engineers realized arches, made of wood or wrought iron (elastic), while masonry (rigid). Already in the 1860’s several elastic analysis of masonry arches were undertaken (for example by the Spanish engineer and architect Saavedra). Some masonry bridges had Castigliano’s [80] theory of elastic systems applied to them. The contribution of Winkler was fundamental in the application of the elastic equilibrium approach to

masonry arch analysis. He studied all the contemporary theories, and comes to the conclusion that elastic analysis was the best choice [81]. He proposed that the "Störungen" (perturbations) can alter the position of the line of thrust. The roots of these perturbations were: possible deformation of the centering during construction, temperature fluctuations, yield of the buttresses under the thrust. Cracks in the arch will be the results of such perturbations, therefore affecting the position of the line of thrust, which could be very different from the calculated (elastically). Winkler, then, suggested a method of controlling the position of the line of thrust by the use of internal hinges during the building phase. Thanks to Winkler elastic analysis appears to be more logical. Three principal points are to be considered [82]:

- stating the equilibrium equations;
- elastic equations are formulated, which compare how the internal forces correspond to deformations of the structure (for example, the bending moment is proportional to the curvature);
- the compatibility of deformation is assumed (affirmations about the way the elements are connected and about the boundary conditions: for example, that the abutments of the arch are flush).

By solving the resulting set of equations a unique, elastic, solution is obtained. Using some admissible values stresses are calculated and compared with some obtained by dividing the exerted forces of the material obtained in laboratory tests.
It is important to bear in mind the resultant system of equations are very sensitive to small fluctuations in the boundary conditions.
We now move on to a masonry arch over a centering. After decentering the arch starts to push against the abutments, which are not rigid and they will give a little. The span naturally increases and the arch must fit into this enlargement of the span. There is one way in which the arch can do this. A fissure opens at the keystone (downwards) and two other fissures open at the abutments (upwards).
The arch has three cracks and a unique line of thrust is possible. Possibly the movement is not even: perhaps the right abutment could yield horizontally, as well as vertically. Each movement creates cracking, and these fissures open and close to allow the arch to resist the forces, it is subject to. The cracking creates the position of the line of thrust. The internal forces change completely due to variations of the formations of the fissures and consequently the thrust line moves abruptly from one position to another. Both large and small fissures produce the same effects regarding the movement of the thrust line. These types of perturbations are impossible to predict, as is the actual line of thrust. We know the line of thrust has to be contained in the thickness of the arch. The minimum thrust and the maximum thrust are the two extreme positions of the thrust line, which corresponds to, as it is evident in the

Figure 17. The cracks behave like hinges and this concept of "hinge" is fundamental to the behavior of masonry structure. Deformations result from the division of the structure in to several parts which, linked via the hinges, allow a certain amount of movements. Cracks are not always dangerous, but collapse of the structure may result from displacements of the abutments.

a) b)

Figure 17: a) Arch in equilibrium condition; b) arch in in incipient collapse with displacements of the abutments.

2.2.1 Limit analysis of masonry arches

Heyman [12] stated explicitly three of the basic assumptions necessary to understand the limit analysis of masonry arches:

- Stone has no tensile strength: this is almost exactly true in this kind of structures, made up of voussoir laid either dry or with very weak mortar: although stone itself may have some tensile strength, the joints will not, therefore no tensile forces can be transmitted from one voussoir to another.
- Sliding failure cannot occur: in fact, friction between voussoirs is high enough to suppose that they cannot slide on one another. Besides, shear forces are low.
- The compression strength, can be supposed to be infinite: as we can see from the analysis of existing bridges, stresses are low enough not to allow crushing of the material. This observation is equivalent to the assumption that stone has an infinite compressive strength.

Based on these assumptions, an important point is the definition of a thrust line for a masonry arch. It can be define within the arch if this arch will have at least one possibility to remain “in one piece”. This does not suggest that the arch will always stand nor does it demonstrate that the arch will collapse, as there is always the chance that slight movement will cause cracks leading to collapse.

In this context, working with the assumption that it was enough to design the structure with a certain degree of safety, Rankine [83] said that an arch would be safe if it is possible to draw a line of thrust within its middle-third. Therefore, it was

enough to design the structure, following this approach to obtain a certain degree of safety. Many bridges and buildings designed in such a way remained sound for decades or centuries.

The theory of limit analysis and the demonstration of the fundamental theorems brought the solution to the problem in the XXth with Gvozdev [84] that refer this study to Heyman's approach. In particular, the Safe Theorem affirms that: "*If a line of thrust can be found which is in equilibrium with the external loads and which lies wholly within the masonry, then the structure is safe"*. In the case of the masonry arch, any line of thrust compatible with the applied loads will satisfy the equilibrium conditions. Therefore, it is possible to draw a line of thrust (equilibrium) within the arch (no-tension material) which proves absolutely that the arch is stable and that collapse will happen. The Safe Theorem has been successfully applied in a vast number of engineering problems in practice. Therefore, finding the actual line of thrust can be solved by the Safe Theorem of Limit Analysis.

2.2.2 The Safe Theorem

We can refer to Heyman's Safe Theorem as it is the theoretical basis for several ways of calculating methods in the analysis of masonry vaults.

Assuming that a few conditions on the material behaviour are satisfied, we can use the theorem to calculate the existence of an internal force system which equilibrates the external loads and guarantees that the masonry structure is in a stable equilibrium state. The assumptions here are that the stone blocks have infinite compressional resistance, and the contacts between them resist only compression and friction, Heyman also assumed that the blocks are rigid. In this way the same equal geometry of the structure is valid for any type of force system which the structure can equilibrate.

Using these calculations, Heyman thus stated the Safe Theorem for masonry arches: ''The structure is safe if a line of thrust can be found which is in equilibrium with the external loads and which lies completely within the masonry".

The Safe Theorem has been successfully applied in a great number of engineering problems, with particular to arches and vaults.

It was widely accepted that Plastic Limit Analysis can be used to check if the structure stands in the given geometry under its own weight in the stability analysis of arches and vaults.

2.2.3 Collapse mechanisms

The collapse of arches should be studied if we are to understand completely masonry arch behaviour. But, we must ask ourselves how is it possible that a structure built

with extremely strong material can collapse. A catastrophic deformation can cause collapse, possibly with no movement of the abutments. When the line of thrust reaches the limit of the masonry a "hinge" forms, which permits rotation (Figure 18). An arch is statically determined by the three hinges, which form the arch and keep the structure stable. An extra hinge converts the arch into a four-bar mechanism leading to collapse. Increasing the load will form four hinges and cause collapse without destroying the material. This can occur in an unstable arch with the addition of extra load, which sufficiently deforms the line of thrust. This process is clarified by the hanging chain analogy.

The standard capacity of masonry is measured by the ultimate limit state. That said, the ultimate limit state of a wall is univocally defined by the kinematic mechanism of collapse, expressed by the form, and by the associated load, the said load of the mechanism. The mechanism load must therefore exceed the extreme load: this is the required verification of masonry structures. The statement concerns any masonry - vestments, columns, vaults - as long as they are in natural conditions; while it does not apply to masonry reinforced by resistant external contributions traction, where the ultimate load may not be a mechanism.

Kooharian defines the concept of collapse with the “unsafe theorem”. In fact a state of collapse can be found if a kinematically admissible condition exists. The kinematically admissible condition is characterized by the state in which the work done by the external loads is greater or equal than to the work of internal forces.

Figure 18: Main kinematic schemes.

2.3 R-adaptive finite element model

In this part, we report a hint of the finite element modeling used in continuous approaches. Specifically, this type of continuous approach typically make use of stress-function formulations of the equilibrium problem that minimize the tensile stress in the masonry elements.

To assess the quality of the finite element solution, we must apply the mesh-adaptive method. Using this method, the computational cost of large-scaled structures may be reduced . The mesh-adaptive method may be classified into h-, p-, and r-adaptive

method. Unlike the first two which increase the cost of the solution, the r-adaptive method technique does not increase the computational cost of obtaining a solution since it introduces no new additional nodes and does not increase the degree of the element basis functions. A stable number of mesh points in a constant connectivity structure is redistributed so that the fine-scale features of interest are best resolved in this approach. A powerful solution for doing this is to move the points so that the point density is controlled by equidistributing an appropriate scalar or matrix monitor function.

Genetic/evolutionary algorithms are particularly useful in structural optimization problems according to a number of studies. In particular, the funicular shapes of curved structures which provide minimal compliance configurations are revealed by such optimization strategies [85]. In the 1960s and optimization through evolutionary algorithms was first developed and now refers to a family of probabilistic search methods inspired by the principle of natural selection [86][87]the solution space is multidimensional, multimodal, discontinuous, and noisy [88]. We deal with a r-adaptive finite element approach to the search for a 'safe' thrust surface of a masonry dome, which is either unreinforced, or reinforced through externally bonded Fiber Reinforced Polymer (FRP) and/or Fabric Reinforced Cementitious Mortar (FRCM) systems over a portion of the boundary by a Breeder Genetic Algorithm (BGA). This is a specific type of evolutionary optimization algorithm, that uses a both stochastic and a deterministic selection scheme, in that the fittest "individuals" (solutions) are selected from a current generation and enter the "gene pool" to be recombined and mutated as the basis to form the new generation, a fitter population, and arrive at an optimal solution [89][90]. It is assumed that the dome resists the external loads through a thrust surface contained in a given search domain, which exhibits zero or almost-zero tensile stresses over the unreinforced portion of masonry. An elastic finite element model is permitted to move within the search domain, utilizing a BGA to manipulate the coordinates of the mesh nodes within the prescribed bounds, and minimizing the maximum tensile stress suffered by the unreinforced masonry (fitness function).

The proposed method is able to deals with arbitrary loading conditions, structural inhomogeneity (e.g., no uniform material properties), and geometries. The modeling of FRP/FRCM reinforcements is carried out following Baratta and Corbi [50][51] by permitting the thrust surface to move outside the physical area of the structure corresponding to the reinforced regions. A benchmark example allows us to emphasize the technical potential of the proposed method, which allows to design

optimal positioning of FRP/FRCM reinforcements, and the resulting benefits with reference to crack damage prevention and the load bearing capacity of the structure.

2.3.1 Numerical model

The proposed numerical procedure is formulated within Heyman's safe theorem, by assuming the structural response of a masonry vault through a compressive membrane state across a material surface S (thrust surface), contained in vault volume.

The hypotheses of the modelling are:

- no tensile strength of masonry;
- infinite compressive strength of masonry;
- sliding failure does not occur.

The last assumption requires values of friction between blocks of the order of 0.5–0.6.At least a thrust surface can be found if the equilibrium of vault under external loads exists. The thrust surface is searched through the refinement adaptive FEM described below, driven by a minimization procedure of tensile stresses by means of a BGA. Such an adaptive FEM allows to approximate the no-tension model of masonry, starting from a FEM model of vault developed within the linear elasticity via shell elements with dominant membrane behaviour (Figure 19). Let denote the i-th coordinate of the j-th node, xi,j; the lower bound of xi,j (corresponding to the intrados of the vault for unreinforced masonry), xi,jmin; the upper bound of xi,j (corresponding to the extrados of the vault for unreinforced masonry), xi,jmax; control variables ranging in the interval [0,1], ξi,j.

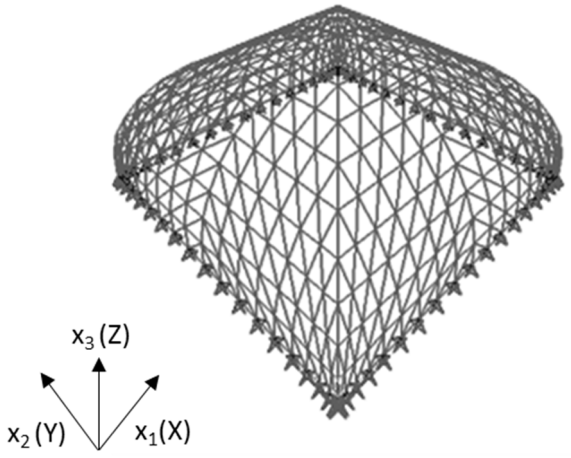

Figure 19: FEM modelling [113].

Let denote the i-th coordinate of the j-th node, xi,j; the lower bound of xi,j (corresponding to the intrados of the vault for unreinforced masonry), xi,jmin; the upper bound of xi,j (correspond-ing to the extrados of the vault for unreinforced masonry), xi,jmax; control variables ranging in the interval [0,1], ξi,j.

We search a safe thrust surface of vaults by moving FEM nodes within a design domain, expressed as follows:

$$\boldsymbol{x_{i,j} = x_{i,j}^{min} + \xi_{i,j}\left(x_{i,j}^{max} - x_{i,j}^{min}\right)}$$

by minimizing the fitness function corresponding to the average value of the principal tensile stresses in unreinforced masonry.

More specifically, if we assume n and N (=3 n if all the 3 nodal coordinates governing the r-adaptation strategy) are the total number of the FEM nodes and control variables $\xi_{i,j}$, respectively, we can introduce the m-th "individual" corresponding to the t-th generation:

$$\boldsymbol{x_m^t = (x_{1,1}, \dots\dots, x_{3,n})_m.}$$

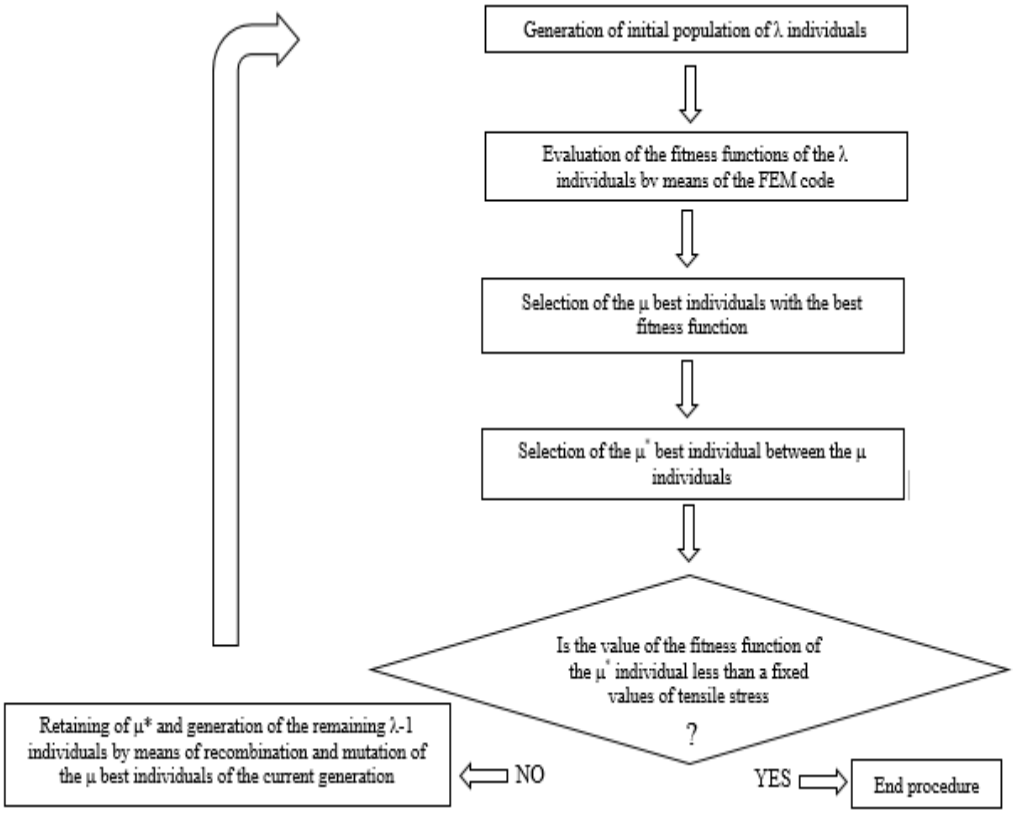

Figure 20: BGA's flow chart [113].

The BGA find the safe thrust surface by performing the following steps (Figure 20):

1. an initial population of λ individuals is generated;
2. the μ best individuals are selected within the current population of λ elements;
3. the best individual is retained for the next generation;
4. the remaining λ-1 individuals of the next generation are created by means of the Extended Intermediate Recombination (EIR)[90] and mutation the μ best individuals of the current generation;
5. Steps 2 through 4 are repeated until the value of fitness function is less than a fixed value of tensile stress.

The proposed procedure allows us to approximate the elastic no-tension constitutive model of unreinforced masonry within a linear elastic FEM analysis.

2.3.2 Validation

The procedure was validated by considering the masonry vault studied by D'Ayala and Tomasoni [91] with span of 6 m, rise of 3 m and thickness of 0.12 m, subject only to self-weight. The mechanical properties of the material are indicated in Table 1 (γ_1 = specific weight of masonry, E_m = Young modulus of masonry).

Table 1 – Main mechanical properties of the materials

γ_1 (kN/m^3)	E_m (MPa)
18.14	5000.00

The comparison between the mechanical response obtained by the proposed procedure and the predictive behaviour of D'Ayala and Tomasoni [91] is performed in terms of thrust surface and natural arches formation.

Let consider an eighth of the vault, by accounting the symmetry of the vault geometry and the loads, and let divide it in four slices (Figure 21,a).

D'Ayala and Tomasoni shown the cloister vault is characterised by the formation of two plastic hinges at the 3rd and 4th slices of the vault. The first one is located at the vault intrados for an angle of 70 with respect to the vertical direction, while the second one is located at the vault extrados for an angle of 30° with respect to the vertical direction.

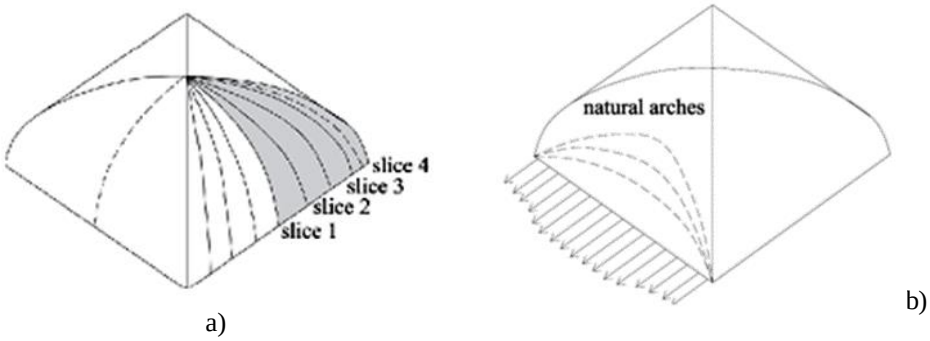

a) b)

Figure 21: (a) Slices definition and (b) natural arches in the limit analysis solution [48].

The authors also highlighted the natural arches configuration of the vault in the limit analysis solution (Figure 21,b). The thrust surface obtained by the proposed procedure allows predicting the hinges formation above mentioned (Figure 22, Figure 23) procedure is also capable to describe the natural arches mechanism, accounting the distribution of the minimum principal internal forces (Figure 24). We denote 'RTS' the Reference Thrust Surface corresponding to the midsurface of the cloister and 'MTTS' the Minimum Tension Thrust Surface obtained via the proposed numerical procedure.

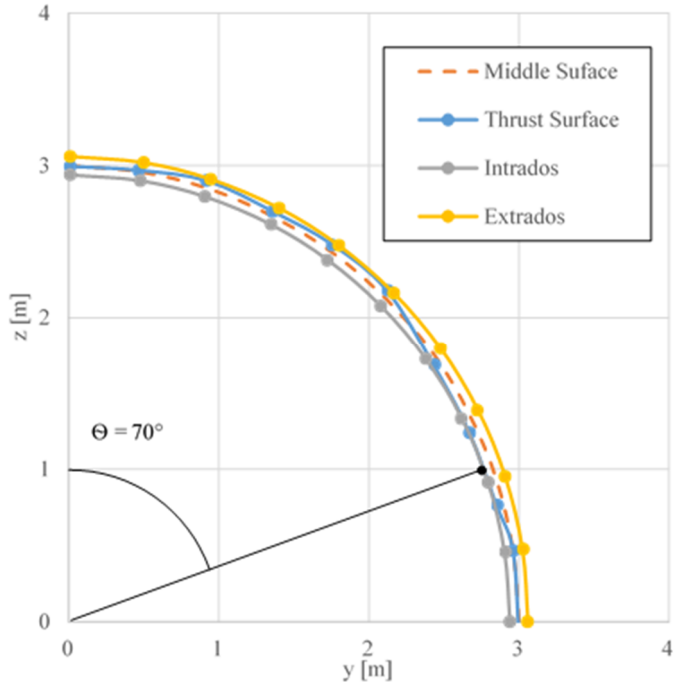

Figure 22: Thrust surface section at centroid of the 3rd slice [113].

The maximum and minimum principal stresses associated to RTS are: σ_{max} = 4.29 x 10^{-1} MPa, σ_{min} = - 4.12 x 10^{-2} MPa, respectively, and the average value of tensile principal stresses are equal to: σ_{ave} = 3.76 x 10^{-8} MPa.

The MTTS gives the maximum principal stress (σ_{max} = 9.00 x 10^{-2} MPa) and the average value of the tensile principal stresses (σ_{ave} = 1.14 x 10^{-8} MPa) considerably smaller than that obtained by the RTS. On the contrary, the minimum principal compressive stress of the MTTS (σ_{min} = -3.73 x 10^{-2} MPa) exhibits a negligible variation if compared to that given by the RTS (Figure 24).

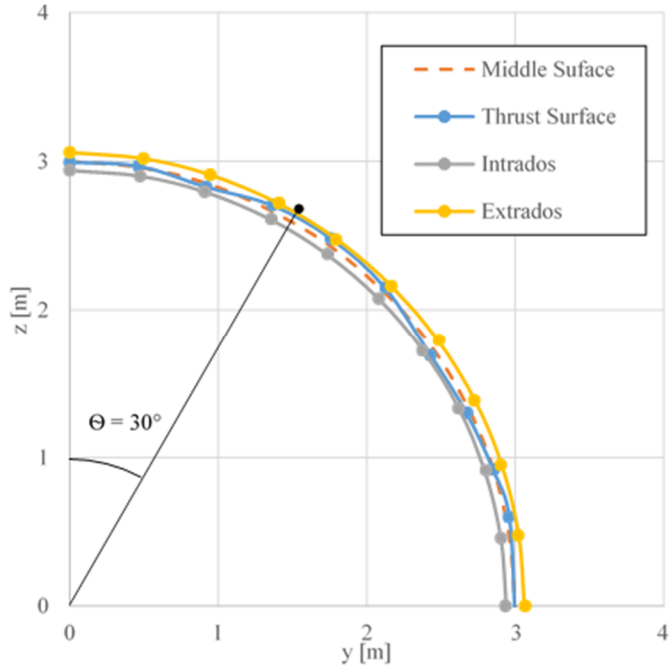

Figure 23: Thrust surface section at centroid of the 4rd slice [113].

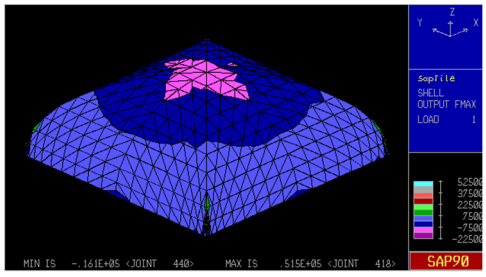

RTS: maximum principal internal forces [N/m]

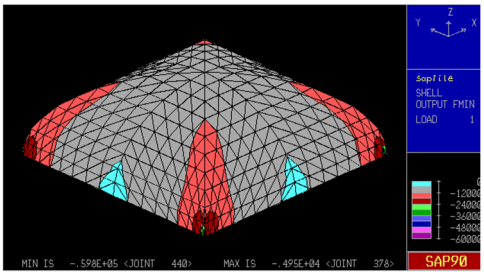

RTS: minimum principal internal forces [N/m]

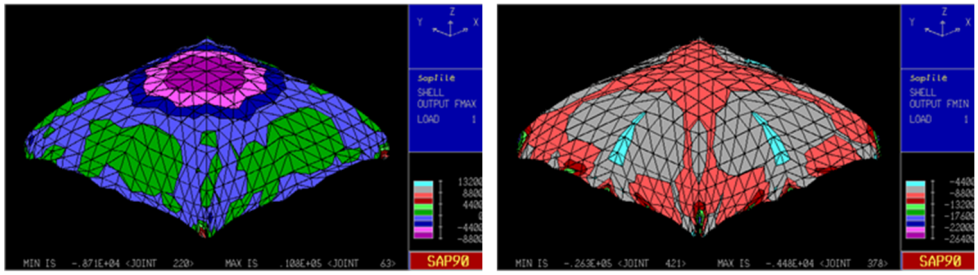

MTTS: maximum principal internal forces [N/m]

MTTS: minimum principal internal forces [N/m]

Figure 24: Views of the unreinforced vault subject to its self-weigh [113].

2.3.3 Case study

We analyze a tuff masonry cloister vault subject to static and dynamic loads.

The cloister vault, as well known, is generated by the intersection more barrel vaults set on opposite sides of a base polygon. The stress state in this kind of vault is more complex than that exhibited by groin and barrel vaults.

The examined vault is characterized by the constant thickness of 0.25 m and its geometry is depicted in Figure 25.

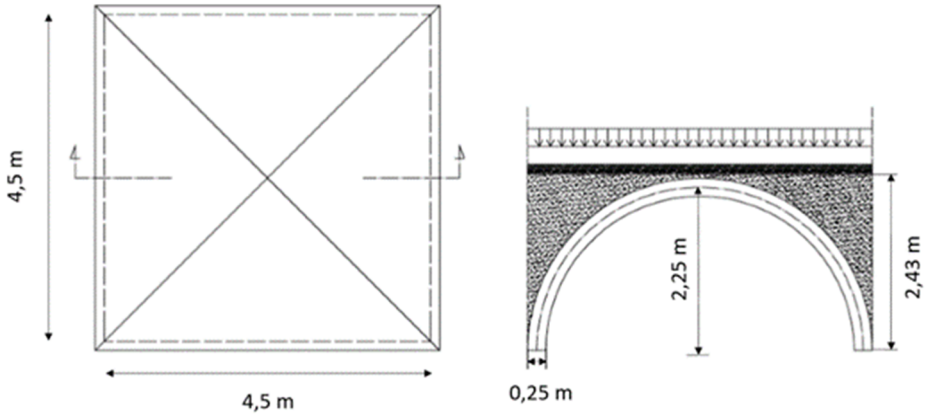

Figure 25: Plan and section of the cloister vault [113].

The masonry framework is modelled, within the numerical procedure, by means of the SAP90 FEM code. The mesh consists of 441 nodes and 800 triangular shell elements with dominant membrane thickness (Figure 26).

We assumed the physical and mechanical properties of the materials, reported in Table 2 (γ_2 = specific weight of filling material). The basis of the cloister vaults is restrained by fixed hinge supports.

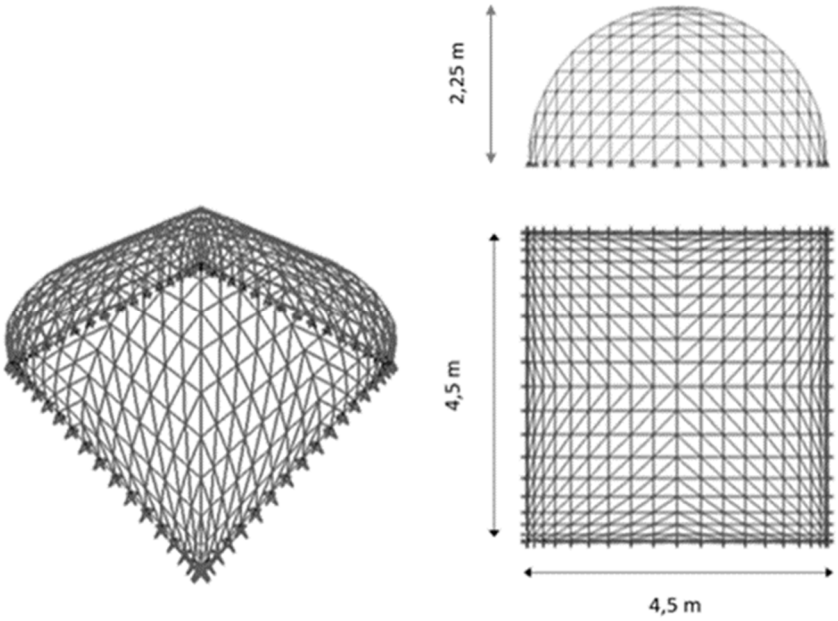

Figure 26: *3D, front and top views of the finite element modelling [113].*

Table 2 – Physical and mechanical properties of the materials

γ_1 (kN/m^3)	γ_2 (kN/m^3)	E_m (MPa)
15.00	10.00	1500.00

We consider three static case studies:

- cloister vault subject to its self-weight - SF;
- cloister vault subject to the dead and live loads - DL;
- cloister vault subject to the dead and half side live loads - DHL.

We also examine the vault under the load combination obtained by vertical and seismic loads.

The seismic action is modelled according to static approach suggested in European Standard EN 1998-1 [92]. In particular, horizontal forces in the *X* direction are set 0,50 of vertical forces (corresponding to the action of dead and live loads).

Finally, we propose a strengthening intervention with FRCM composites of the vault and we study the mechanical behaviour of the reinforced vault.

Within numerical simulations, the fitness function is applied to unreinforced masonry; the relocating of FEM nodes of the unstrengthen masonry is allowed along

the Z-axis of the Cartesian frame within the vault volume; the relocating of FEM nodes of reinforced masonry is allowed along the Z-axis beyond the physical domain of the structure for the FRCM regions, on the opposite side of the reinforcements. Plots of maximum and minimum principal internal forces are given in the following, referred to the RTS and the MTTS.

2.3.4 Unreinforced vault

2.3.4.1 Self-weight - SF

Firstly, we apply the numerical model to the vault subject to its self-weight. Starting from the FEM analysis on the RTS and the MTTS, the maximum and minimum internal forces acting on midsurface of shell elements are obtained (Figure 27).
In terms of local stresses, the maximum and minimum principal stresses on the RTS are equal to σmax = 3.04 x 10-2 MPa and σmin = - 4.40 x 10-2 MPa, respectively, and the average value of the tensile principal stresses is equal to σave = 3.73 x 10-9 MPa.
In terms of local stresses, the maximum and minimum principal stresses on the RTS are equal to σ_{max} = 3.04 x 10^{-2} MPa and σ_{min} = - 4.40 x 10^{-2} MPa, respectively, and the average value of the tensile principal stresses is equal to σ_{ave} = 3.73 x 10^{-9} MPa.

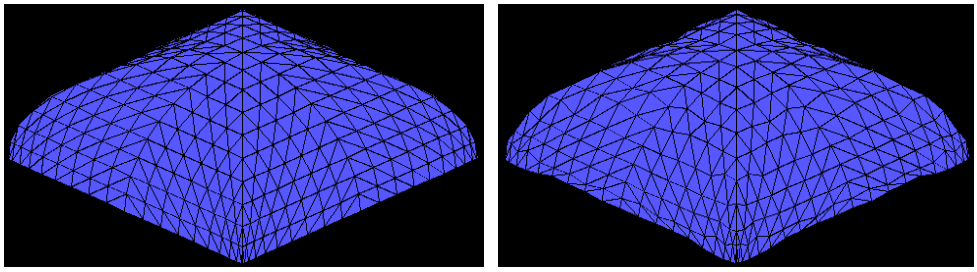

Figure 27: *Plan and section of the cloister vault*

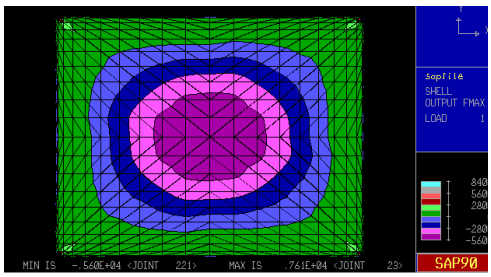

RTS: maximum principal internal forces [N/m]

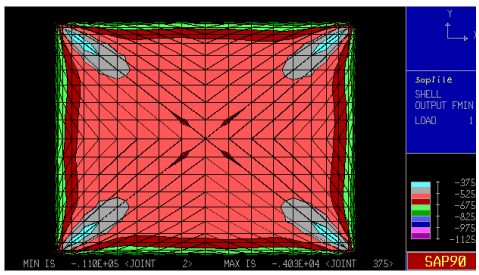

RTS: minimum principal internal forces [N/m]

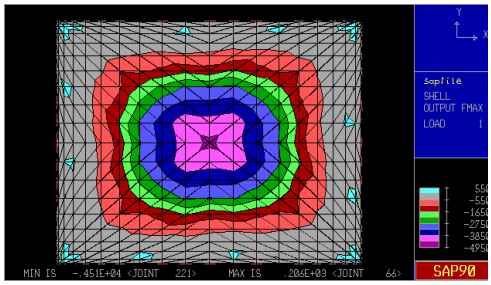

MTTS: maximum principal internal forces [N/m]

MTTS: minimum principal internal forces [N/m]

Figure 28: *Top views of the unreinforced vault subject to its self-weight [113].*

The results obtained by considering the MTTS highlight the maximum principal stress (σ_{max} = 8.24 x 10^{-4} MPa) and the average value of the tensile principal stresses (σ_{ave} = 5.35 x 10^{-10} MPa) are significantly smaller than that obtained by the RTS, and the minimum principal compressive stress given by the MTTS (σ_{min} = - 4.08 x 10^{-2} MPa) is almost unchanged compared to that given by the RTS (Figure 28).

2.3.4.2 Dead and live loading - DL

Let us examine the vault subject to the following static design load combination, LC_{St}:

$$\boldsymbol{LC_{St} = G_1 + (G_{2,1} + G_{2,2}) + Q}$$

where:

- G_1 is the dead load due to the self-weight of the vault;
- $G_{2,1}$ is the dead load due to the weight of the filling material;
- $G_{2,2}$ is the dead load due to the permanent overload and it is assumed equal to 3.00 kN/m^2;
- Q is the live load ad it is fixed equal to 4.00 kN/m^2.

The FEM analysis referred to the RTS and the MTTS of Figure 29 gives the maximum and minimum internal forces acting on midsurface of shell elements.

The corresponding maximum and minimum principal stresses on the RTS are equal to σ_{max} = 1.03 x 10^{-1} MPa and σ_{min} = -1.40 x 10^{-1} MPa, respectively, and the average value of the tensile principal stresses is equal to σ_{ave} = 1.26 x 10^{-8} MPa.

The MTTS allows to point out the maximum principal stress (σ_{max} = 7.20 x 10^{-3} MPa) and the average value of the tensile principal stresses (σ_{ave} = 3.01 x 10^{-9} MPa) are significantly smaller than that obtained by the RTS, and the minimum principal compressive stress given by the MTTS (σ_{min} = -1.42 x 10^{-1} MPa) remains almost unchanged in magnitude compared to that given by the RTS (Figure 30).

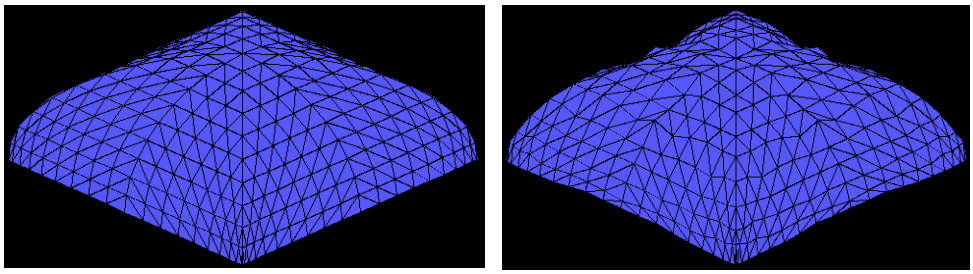

Figure 29: *Top views of the unreinforced vault subject to dead and live loads*

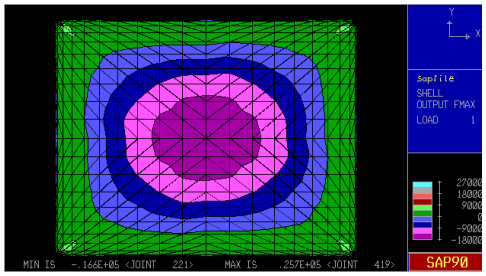

RTS: maximum principal internal forces [N/m]

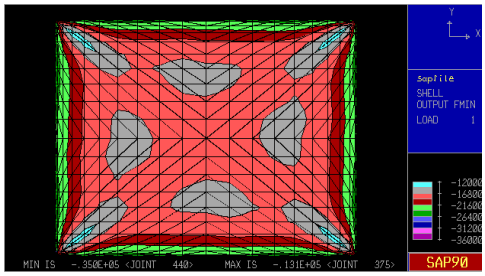

RTS: minimum principal internal forces [N/m]

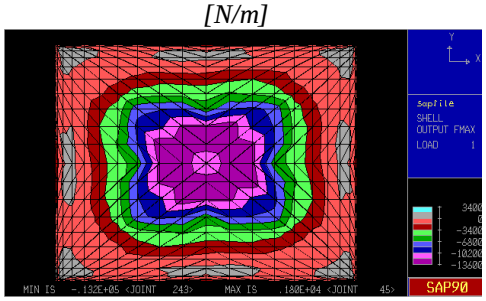

MTTS: maximum principal internal forces [N/m]

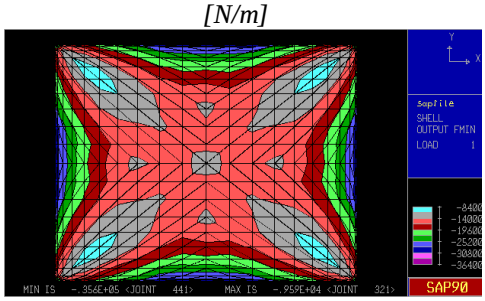

MTTS: minimum principal internal forces [N/m]

Figure 30: *Top views of the unreinforced vault subject to dead and live loads [113].*

2.3.4.3 Dead and half side live loading - DHL

The vault is analyzed under the LC_{St} combination of the previous case, by assuming half side live loads (Figure 31). The MTTS is obtained starting from the RTS (Figure 14) and the corresponding membrane stress maps are depicted in Figure 32.

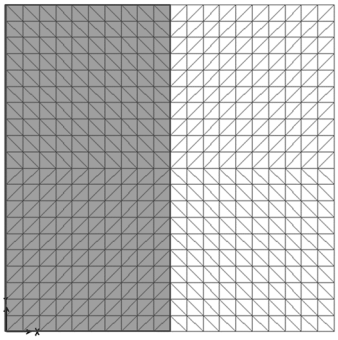

Figure 31: *Plan of the live loads (the live loads are applied on the grey surface [113].*

The RTS gives the maximum and minimum principal stresses of 8.08 x 10^{-2} MPa and -1.18 x 10^{-1} MPa, respectively. The corresponding average value of the tensile principal stresses of 1.03 x 10^{-8} MPa is also obtained.

The results show the maximum principal stress (σ_{max} = 6,04 x 10^{-3} MPa) and the average value of the tensile principal stresses (σ_{ave} = 2.75 x 10^{-9} MPa) of MTTS, which are significantly smaller than that obtained by the RTS. The minimum principal compressive stress given by the MTTS (σ_{min} = -1.18 x 10^{-1} MPa) is almost unchanged compared to that given by the RTS (Figure 33).

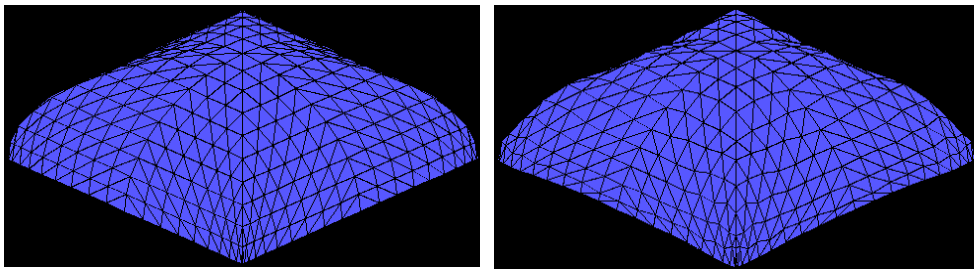

Figure 32: *RTS and MTTS configurations*

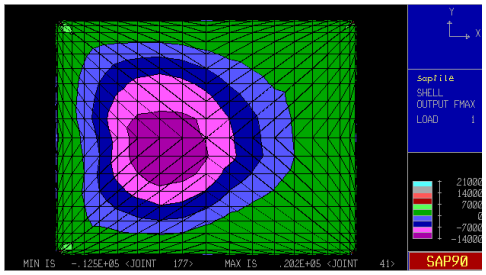

RTS: maximum principal internal forces [N/m]

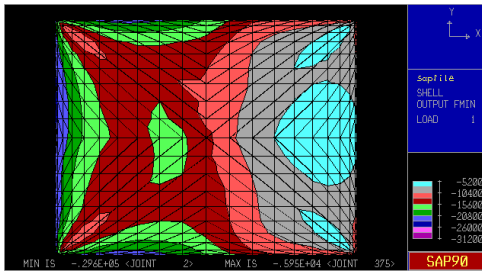

RTS: minimum principal internal forces [N/m]

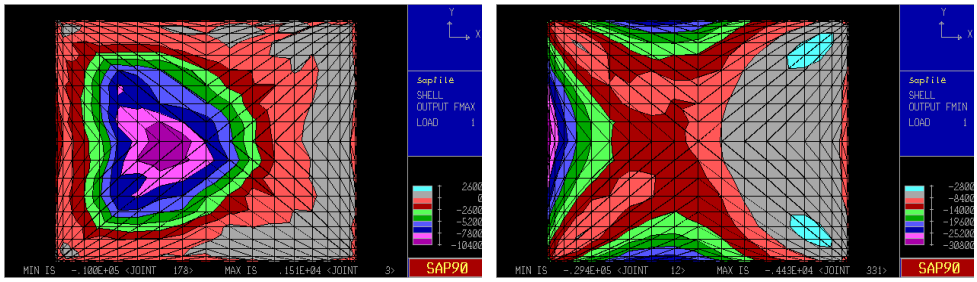

MTTS: maximum principal internal forces [N/m] *MTTS: minimum principal internal forces [N/m]*

Figure 33: Top views of the unreinforced vault subject to dead and half side live loads [113].

2.3.5 Reinforced vault

2.3.5.1 Seismic loading and strengthening with FRCM strips

Let us examine the vault subject to the following dynamic design load combination, LC_{Dyn}:

$$\boldsymbol{LC_{Dyn} = E + G_1 + (G_{2,1} + G_{2,2}) + \psi_{2,1} Q}$$

where:

- E is a the load due to the seismic excitation along the X-axis of the Cartesian frame;
- G_1 is the dead load due to the self-weight of the vault;
- $G_{2,1}$ is the dead load due to the weight of the weight of filling material;
- $G_{2,2}$ is the dead load due to the permanent overload and it is assumed equal to 3,00 kN/m2;
- $\psi_{2,1}$ is the combination coefficient and it is assumed equal to 0,80;
- Q is the live load ad it is fixed equal to 4,00 kN/m2.

The effects of the seismic excitations are modeled by means of horizontal forces according to a conventional static approach to seismic actions on the buildings (European Standard EN 1998-1) [93]. The seismic actions are set 50% of the vertical forces.

The RTS and the obtained MTTS are reported in Figure 34 and the corresponding maps of the maximum and minimum internal forces are shown in Figure 35. The maximum principal stresses on the RTS and the MTTS are equal to σ_{max} = 3.50 x 10^{-1} MPa and σ_{max} = 1.50 x 10^{-1} MPa, respectively; the minimum principal stresses on the RTS and the MTTS are equal to σ_{min} = - 4.28 x 10^{-1} MPa and σ_{min} = - 5.28 x

10^{-1} MPa, respectively; and the average values of tensile principal stresses are equal to σ_{ave} = 4.00 x 10^{-8} MPa and σ_{ave} = 2.65 x 10^{-8} MPa, respectively.

It is worth noting that, also in this simulation, a relevant reduction of the maximum tensile principal stresses (56 %) can be obtained by considering the MTTS as an alternative configuration to the RTS.

The FEM analysis on the MTTS has highlight, close to the vault basis, the principal tensile stresses are comparable to the tensile strength of tuff masonry (1.00 x 10^{-1} MPa) and the corresponding principal directions are roughly horizontal.

Therefore, a selective strengthening intervention with composite materials is proposed.

More specifically, commercial unidirectional FRCM strips is considered, whose mechanical properties are given in Table 3.

We assume to place the reinforcement at the extrados, close to the vault basis subject to principal tensile stresses comparable to the masonry tensile strength, and the fibre orientation parallel to the vault basis.

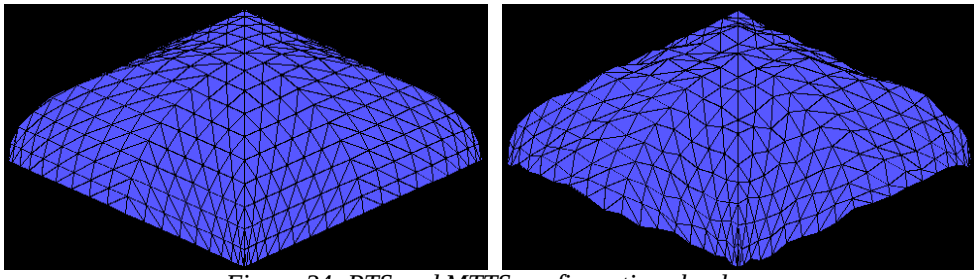

Figure 34: RTS and MTTS configurations loads

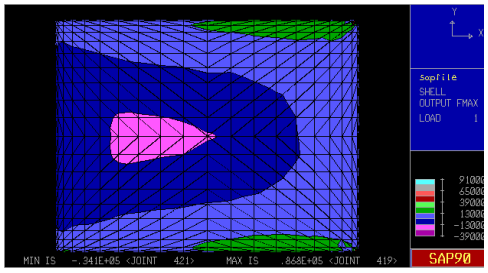

RTS: maximum principal internal forces [N/m]

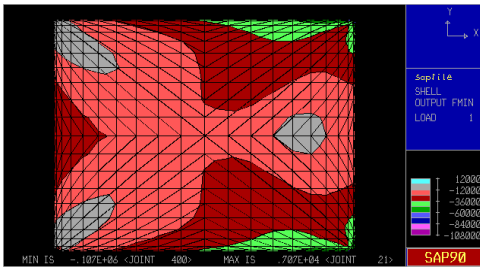

RTS: minimum principal internal forces [N/m]

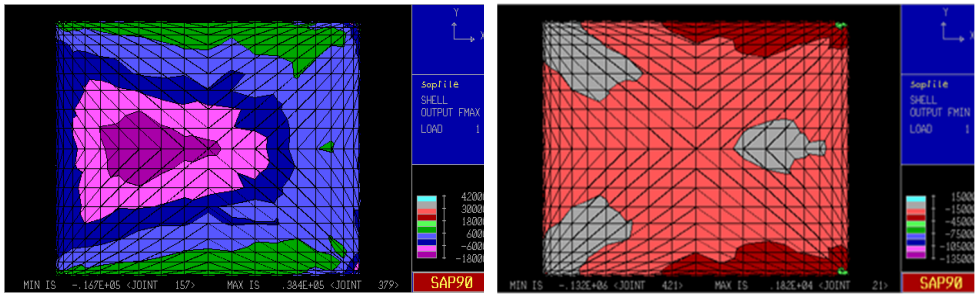

MTTS: maximum principal internal forces [N/m]

MTTS: minimum principal internal forces [N/m]

Figure 35: Top views of the unreinforced vault subject to seismic loads [113].

The FEM analysis on the MTTS of the reinforced vault (Figure 36), gives the maximum and minimum internal forces acting on midsurface of shell elements (Figure 20). The corresponding maximum tensile stresses in unreinforced masonry are less than the tensile strength of tufa masonry.

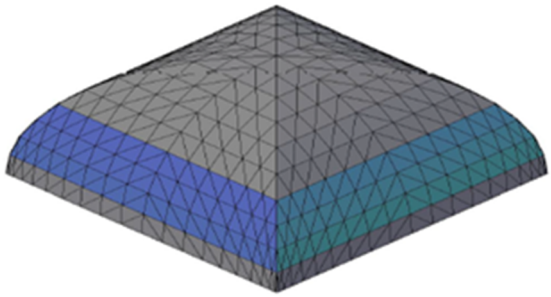

Figure 36: 3D views of the reinforced vault (the FRCM strips are applied on the blue surface)[113].

Table 3 – Mechanical properties of FRCM

Carbon fiber			
Tensile strenght (MPa)	Young modulus (GPa)	Density (g/cm^3)	Ultimate strain (%)
4800	240	1.82	13.30
Cementitious Matrix			
Compressive strenght (MPa)	Flexural strenght (MPa)	Young modulus (MPa)	
≥ 20.0 (after 28 d)	≥ 3.5 (after 28 d)	≥ 7000 (after 28 d)	

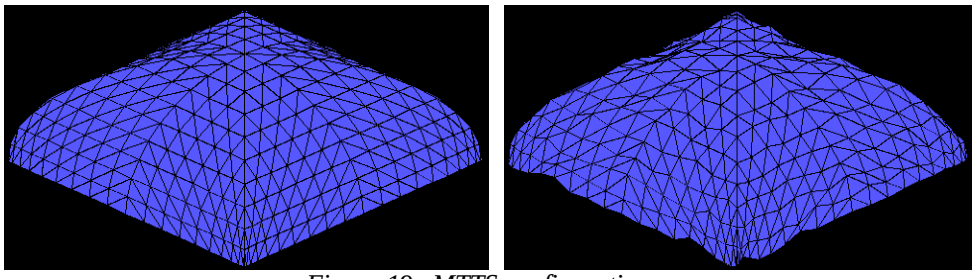

Figure 19– MTTS configuration.

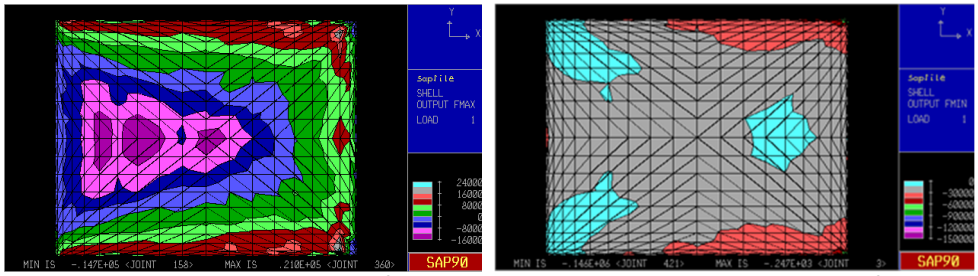

MTTS: maximum principal internal forces [N/m]

MTTS: minimum principal internal forces [N/m]

Figure 37: Top views of the reinforced vault subject to seismic loads of 'MTTS' configurations [113].

Part III. Discrete Approaches

In this Part of the thesis we investigate computational approaches that describe particle interactions in discrete systems. Two approaches are presented as useful tools for the evaluation of the stability of vaulted masonry structures. Specifically, they aim to highlight an optimal form and mass strategy, by defining a lattice model and respecting the limit analysis theorem.
In the first case, we deal with the description of the Lumped Stress Method (LSM), which is applied to unreinforced masonry structures, under static loads, given by self-weight and distributed or concentrated loads. On the other hand, we use the tensegrity approach to present a topological optimization of the reinforcement of masonry vaults and domes established by meshes of Fiber Reinforced Polymers (FRP) and/or Fabric Reinforced Cementitious Matrix (FRCM), in the case of static and dynamic loads.
From the conceptual point of view, we will see how the two approaches are used as complementary.

3.1 The lumped stress method

The first phase of the research activity carried out for the present thesis work has been oriented towards the formulation of mechanical models and numerical algorithms for the study of the static behavior of vaults and masonry domes.
A "no-tension" mechanical model has been proposed which assumes the formation inside a vaulted wall structure of a resistant surface S (thrust surface) can be subdivided, in more general cases, into a portion subjected to biaxial compression, in a portion subjected to uniaxial compression and in a completely discharged portion.
According to the "no-tension" model, the first one does not experience any fracturing; the second can fracture along the compression isostatic, while the third can fracture along arbitrary directions.
The problem of membranous balance has been referred as a potential of the efforts projected on the base (or platform) of the vault, according to a Pucher approach.
The use of a particular method of variational approximation of the equilibrium problem (of the "non-conforming" type), has led to represent the regime of membrane stresses through a spatial lattice of concentrated efforts.

By virtue of the "isostaticity" of the membranous problem, to every shape of the surface S corresponds one and only one lattice of stress concentrated in equilibrium with the external loads. However, for a generic form of S, balanced efforts do not, in general, satisfy the constitutive constraint of non-tensile strength.
The problem is then reduced to the iterative search for a surface S to which purely compressive stresses correspond and which is contained entirely within the thickness of the solid.

3.1.1 Membrane problem in Pucher approach

The Lumped stress method has basically, adopted the Pucher approach. Such an approach is particular suitable for the formulation of the membrane equilibrium problem.
Convenient systems of coordinates for the formulation of the deformation problem are the Cartesian one for shells of translation and the cylindrical one for shells of revolution. This same choice of coordinates is stated in Pucher's formulation of the membrane stress problem and accounts for the general applicability of this method. In many formal aspects, the present calculation of membrane deformations is an extension of the Pucher method and we therefore begin with a brief review of the latter.

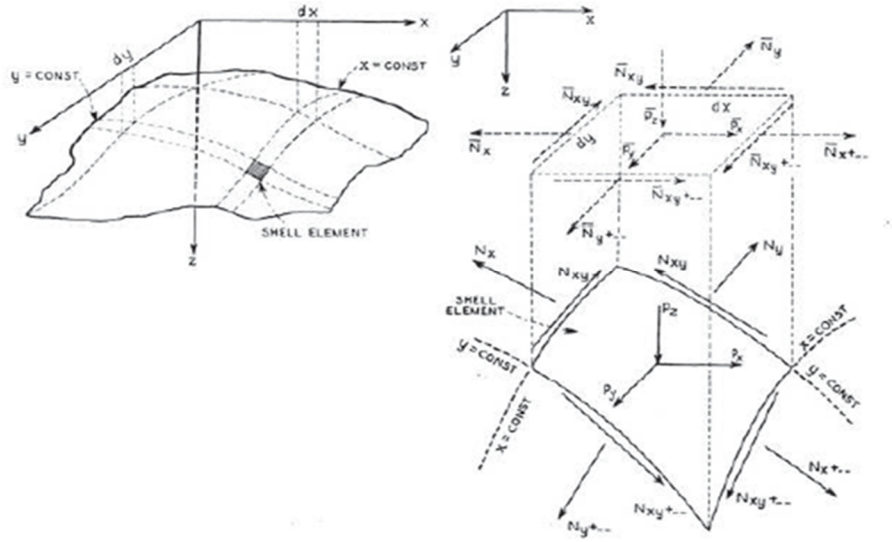

Figure 38: A shell arbitrary configuration whose middle surface is given as z(x,y) in the cartesian system of coordinates (left); magnified view is shown ot a differential element of the shell, this element being bounded by arcs of coordinate lines (right) [114].

Figure 38 (left) shows a shell of arbitrary configuration whose middle surface is given as z (x, y) in the Cartesian system of coordinates. A few coordinate lines x constant and y constant are indicated on it. In Figure 38 (right) a magnified view is shown as element of the shell, this element being bounded by arcs of coordinate lines. It is loaded by the external forces px, py, pz, per unit area of the shell and held in equilibrium by the skew system of membrane forces Nx, Ny, and Nxy per unit length of coordinate line.

The equality of the shear resultants, *Nxy Nyx* readily follows. In the Pucher method we write the equilibrium equations for the shell element in terms of the horizontal components of the membrane forces per unit length of horizontal line element dx or dy, denoted as *Nx, Ny, Nxy,* and shown in fig. 2. Likewise, the external loads are expressed per unit horizontal area of dxdy and denoted as *px, py, pz.* This set of forces will be referred to as the projected forces of the shell element. It is readily seen that the equilibrium equations for the shell element in the x and y directions in terms of the projected forces turn out to be identical to the equilibrium conditions of plane stress or plane strain, namely:

$$\frac{\partial Nx}{\partial x} + \frac{\partial Nxy}{\partial x} = -px; \qquad (1)$$

$$\frac{\partial Ny}{\partial y} + \frac{\partial Nxy}{\partial x} = -py; \qquad (2)$$

The equilibrium equation in the z-direction is:

$$\frac{\partial Nx}{\partial x} z_x + N_x z_{xx} + \frac{\partial Ny}{\partial y} z_y + N_x z_{yy} + \frac{\partial Nxy}{\partial x} z_y + \frac{\partial Nxy}{\partial y} z_x + 2N_{xy} z_{xy} = -pz; \quad (3)$$

by way of further comparison with the plane stress problem, takes the place of the compatibility equation there. As in the plane theory of elasticity, we introduce the Airy stress function φ according to definitions, which satisfies the equilibrium equations (1) and (2) automatically. Equation (3) is left to be satisfied by the stress function and takes the form:

$$L(\varphi) = \varphi_{xy} z_{xx} - 2\varphi_{xy} z_{xy} + \varphi_{xx} z_{yy} = -p_z + p_z z_x + p_y z_y + z_{xx} \int p_x d_x + z_{yy} \int p_y d_{xy};$$

where *L* will be called the Pucher operator.

3.1.2 Variational approach to the equilibrium on masonry valuts

Let us consider a double-curved solid with an elastic behaviour and let us assume that it resists external loads by exhibiting a no tension membrane regime. We can see this surface, as the thrust surface *S* of a masonry vault. It is contained in a design

domain, and its shape function f = $f(x_1, x_2)$. The membrane behaviour is modelled by means of a discrete network of compressive forces, which allows us to approximate the no-tension model of masonry by the Pucher's approach defined above (Figure 39).

Let Ω denote the horizontal projection of the thrust surface and let $\{x_1, x_2, x_3\}$ be Cartesian coordinates with unit base vectors $\{\mathbf{e}_1, \mathbf{e}_2, \mathbf{e}_3\}$, such that x_3 is perpendicular to Ω. The covariant base vectors can be easily obtained by regarding x_1 and x_2 as curvilinear coordinates over S (Monge's coordinates), as follows:

$$\mathbf{a}_1 = \mathbf{e}_1 + \frac{\partial f}{\partial x_1}\mathbf{e}_3, \tag{4}$$

$$\mathbf{a}_2 = \mathbf{e}_2 + \frac{\partial f}{\partial x_2}\mathbf{e}_3, \tag{5}$$

$$\mathbf{a}_3 = \frac{1}{J}\mathbf{a}_1 \times \mathbf{a}_2, \tag{6}$$

Where:

$$J = \sqrt{1 + \left(\frac{\partial f}{\partial x_1}\right)^2 + \left(\frac{\partial f}{\partial x_2}\right)^2}. \tag{7}$$

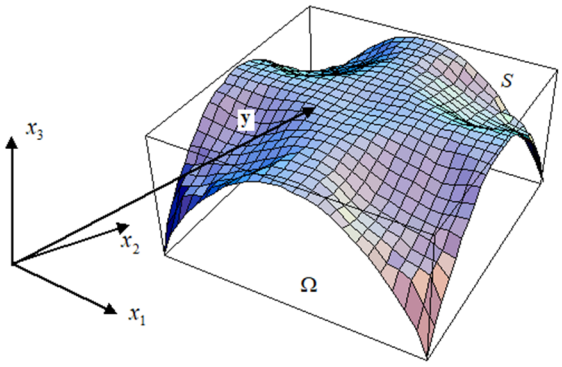

Figure 39: Thrust Surface – S [115].

The equilibrium equations of S are conveniently formulated with reference to the non-orthogonal basis $\{e_1, e_2, a_3\}$:

$$\frac{\partial P^{\alpha\beta}}{\partial x_\beta} + q_{(\alpha)} = 0, \quad \text{(summation on } \alpha, \beta \text{)} \tag{8}$$

$$\frac{\partial^2 f}{\partial x_\alpha \partial x_\beta} P^{\alpha\beta} - \frac{\partial f}{\partial x_\alpha} q_{(\alpha)} + q_{(3)} = 0, \quad \text{(summation on } \alpha, \beta \text{)} \tag{9}$$

Here, $q_{(i)}(i = 1, 2, 3)$ denote the external forces per unit area of Ω acting on S, while $P^{\alpha\beta} = JN^{\alpha\beta}$ $(\alpha, \beta = 1, 2)$ denote the projections of the membrane stress resultants $N^{\alpha\beta}$ onto Ω. The $P^{\alpha\beta}$ stresses can be derived from the Airy potential (or stress function) φ, assuming pure vertical loading ($q_{(1)} = q_{(2)} = 0$):

$$P^{11} = \frac{\partial^2 \varphi}{\partial x_2^2}, \tag{10}$$

$$P^{22} = \frac{\partial^2 \varphi}{\partial x_1^2}, \tag{11}$$

$$P^{12} = -\frac{\partial^2 \varphi}{\partial x_1 \partial x_2}, \tag{12}$$

The equation (9) can be rewritten by substituting equations (10)-(11)-(12), as follows:

$$a_{\alpha\beta} \frac{\partial^2 \varphi}{\partial x_\alpha \partial x_\beta} - q = 0, \text{ in } \Omega \tag{13}$$

Where:

$$a_{11} = \frac{\partial^2 f}{\partial x_2^2}, \tag{14}$$

$$a_{22} = \frac{\partial^2 f}{\partial x_1^2}, \tag{15}$$

$$a_{12} = -\frac{\partial^2 f}{\partial x_1 \partial x_2}, \tag{16}$$

$$q = -q_{(3)}. \tag{17}$$

Once the surface tractions along the boundary of *S* are prescribed, the equation (13) can be solved by considering the boundary condition $\varphi = \mu(s)$ su $\partial\Omega$, in which *s* is a curvilinear coordinate measured along the arc-length of $\partial\Omega$, and $\mu(s)$ (Dirichlet problem) is the moment of all support forces about a vertical axis through the point s.

The stress function φ is obtained via the following variational formulation:

$$\int_{\Omega} a_{\alpha\beta} \frac{\partial\varphi}{\partial x_\alpha} \frac{\partial\delta\varphi}{\partial x_\beta} \, d\Omega \quad + \quad \int_{\Omega} q \, \delta\varphi \, d\Omega = 0, \quad \forall \delta\varphi : \delta\varphi = 0 \; su \; \partial\Omega. \tag{18}$$

The equation (18) has to be satisfied for each $\delta\varphi$ vanishing on $\partial\Omega$.

It is well-known that the no-tension constraint for the masonry implies that φ in addition must be concave [28].

The Airy stress function φ is evaluated by using the constrained LSM approach below presented.

3.1.3 Numerical approximation

The LSM presented in Fraternali [94] and Fraternali et al. [72][73] approximates the Airy stress function φ through piece-wise linear functions φˆ defined over either the shape function, in the case of curved structures, or the plain body, in the case of walls.

The method has been originally developed for curved surfaces, starting from a partially non-conforming scheme [95] formulated under the assumption of C_0

approximations to both f and φ, (i.e., polyhedral test functions f^ and φ^ defined on a triangulation Ω_h of Ω) (Figure 40).

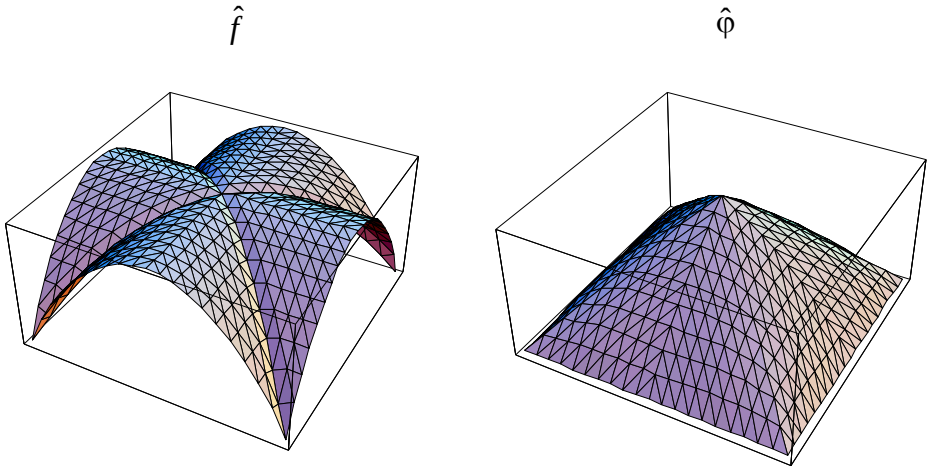

Figure 40: Polyhedral approximations to (a) f and (b) φ [115].

Such an approximation scheme leads to the following discrete version of equation (18):

$$\sum_{lati} \hat{A}_i^j \frac{\hat{\varphi}_j - \hat{\varphi}_i}{h_i^j} (\delta\hat{\varphi}_j - \delta\hat{\varphi}_i) + \sum_{nodi} Q_i \, \delta\hat{\varphi}_i = 0 \qquad (19)$$

Where:

- h_i^j is the length of the edge of Ω_h connecting nodes i and j;
- $\hat{\varphi}_1, \ldots, \hat{\varphi}_N$ are the nodal values of $\hat{\varphi}$;
- $\hat{A}_i^j$ is the jump of the derivative $\frac{\partial \hat{f}}{\partial n}$ along the normal to the edge i-j;
- Q_i is the resultant vertical force in correspondence with node *i*.

The quantity $\hat{A}_i^j$ represents a second derivative in the distributional sense of the polyhedral function $\hat{f}$. Similarly, the jump $\partial\varphi\hat{}/\partial n$ through i-j represents a second generalized derivative of the tensions function $\hat{\varphi}$, that is, on the basis of a singularity of the tension field $\hat{P}^{\alpha\beta}$ associated to $\hat{\varphi}$.

By virtue of this consideration, the various quantities $\hat{P}_i^j = [[\partial\hat{\varphi}/\partial n]]_i^j$ can in fact be regarded as the axial stresses borne by a flat reticular structure Ω_h, having the same geometry as the "skeleton" of the mesh Π_h.

Applying the generalized Gauss formula, from equation (19) we deduce the following system of linear algebraic equations:

$$R_i = \sum_j \hat{P}_i^j \frac{\hat{f}_i - \hat{f}_j}{h_i^j} - Q_i = \sum_{j,k} U_{ijk}\hat{\varphi}_j \hat{f}_k - Q_i = 0 \ , \qquad (20)$$

In equation (20), the quantity *Pij* represents the jump of the normal derivative $\partial\varphi\hat{}/\partial n$ across the edge *i–j* of Ωh; *Uijk* are coefficients depending only on the geometry of the mesh; the summations are extended to all the nodes connected to the node *i*; and *N* is the total number of nodes forming Ωh.

Quantities $\bar{P}_i^j$ are the axial forces carried by the bars of a planar truss structure having the same geometry of the skeleton of Ωh.

One can regard the quantities $\bar{P}_i^j(\bar{f}_j - \bar{f}_i)/h_i^j$ as the axial forces carried by the spatial truss *Sh*, which is obtained from Ωh through the mapping $x_3 = f\hat{}\,(x_1, x_2)$.

Equation (9) represent the nodal equilibrium equations of *Sh* in the vertical direction, associating a unique polyhedral stress function $\varphi\hat{}$ to a given polyhedral shape function $f\hat{}$, and vice-versa. A concave polyhedral stress function $\varphi\hat{}$ gives rise to all compressive forces in the bars of *Sh* and Ωh. It is worth noting that the modelling of a continuous membrane through a pin-jointed bar network actually corresponds to a non-conforming (or external) variational approximation of the membrane equilibrium problem.

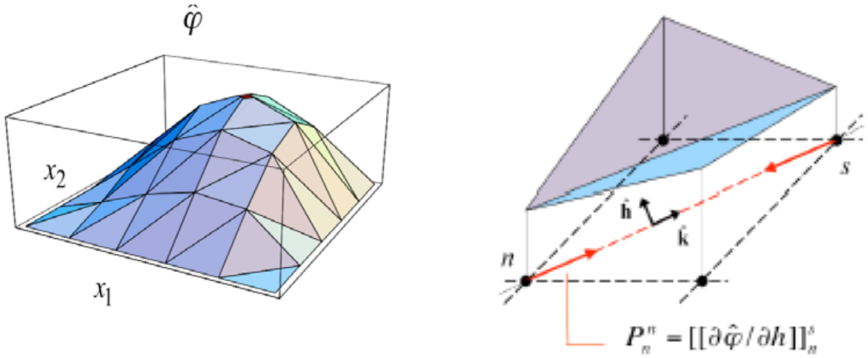

Figure 41: Polyhedral approximation of the Airy stress function and current lumped stress [115].

Let introduce the 'relaxed' version of the complementary energy of the body (Figure 41):

$$E_h(\hat{\varphi}) \;=\; \frac{1}{2}\sum_{n=1}^{N}\sum_{s,t=1}^{S_n}\hat{A}_n^{st}\,P_n^s(\hat{\varphi})\,P_n^t(\hat{\varphi}) \;-\; \sum_{n\in U}\mathbf{R}_n(\hat{\varphi})\cdot\bar{\mathbf{u}}_n\;, \qquad (21)$$

Where:

$$\hat{A}_n^{st} = \frac{\ell_n^s\,\ell_n^t\;\boldsymbol{A}\;[\hat{\mathbf{h}}_n^s\otimes\hat{\mathbf{h}}_n^s]\cdot\hat{\mathbf{h}}_n^t\otimes\hat{\mathbf{h}}_n^t}{4\,|\,\hat{\Omega}_n\,|} \qquad (22)$$

In equations (21)–(22), *N* is the total number of nodes of Π_h; S_n indicates the number of nearest neighbors of the generic node *n*; ℓ_n^s is the length of the edge $n - s$; $\hat{\mathbf{k}}_n^s$ and $\hat{\mathbf{h}}_n^s$ are the tangent and normal unit vectors to such an edge, respectively; $P_n^n = [[\partial\hat{\varphi}/\partial h]]_n^s$ is the jump of $\nabla\hat{\varphi}\cdot\hat{\mathbf{h}}_n^s$ across $n - s$ (i.e., the normal derivative of φ^ through this edge).
It is not difficult to show that:

$$\mathbf{R}_n(\hat{\varphi}) \;=\; -\sum_{s=1}^{S_n} P_n^s(\hat{\varphi})\hat{\mathbf{k}}_n^s\;. \qquad (23)$$

The quantities P_n^s represents the axial forces carried by the bars of an ideal truss B_h which has the same geometry of the skeleton of Π'_h . Similarly, the quantity $\mathbf{R}_n$ can be regarded as the total force acting at node n of such a truss. Due to the assumption of zero body forces, Rn will be non-zero only at the boundary (support reaction). The discrete functional (21) defines a non-conventional complementary energy of the truss B_h, which is defined per dual elements $\hat{\Omega}_n$, and not per elements (as in an ordinary truss).

Let φ0 denote the minimizer of the 'exact' complementary energy of the body, and $\hat{\varphi}_h$ the minimizer of equation (21). It is not difficult to show that $\hat{\varphi}_h$ strongly converges to φ0 as h tends to 0, under suitable smoothness assumptions on φ0 and the primal and dual meshes.

The smoothness of meshes can be satisfied by modelling Π_h as a structured core and by assuming that Π_h is made up of polygons connecting the middle points of the edges of Π_h with the barycenter of the primal triangles ('barycentric' dual mesh). A Γ-convergence proof of the LSM for the bi-harmonic problem of isotropic elasticity is given in Davini [96], considering families of triangulations that are regular in the sense of Ciarlet [95].

3.1.3 Constrained LSM approach to the analysis of curved structures

Lumped stress approach is used to predict the mechanical behaviour of vaulted structures by means of a shape optimization procedure, which assumes that the vertical load q and the boundary values of f^ and φ^ are prescribed on ∂Ωh. The search for the corresponding thrust surface consists of seeking a couple (f^, φ^) such that the discrete equilibrium equation are satisfied, under geometry constraints of the form:

$$\hat{f}_i^{lb} \le \hat{f}_i \le \hat{f}_i^{ub} \quad (i = 1,..., N), \tag{24}$$

and the concavity constraint on φ^. Limitations (24) require that the thrust surface is contained in a given 3D domain D, coinciding either with the region comprised between the extrados and the intrados of an existing vault, or with a suitable design space. A constrained lumped stress approach (CTNA) can be formulated as follows, assuming that initial guess $\hat{f}^0$ of $\hat{f}$ is available:

1. Compute φ^0 from the linear system $\left(U_{ijk}\ \hat{f}_k^{\,0}\right)\hat{\varphi}_j^{\,0} = Q_i$;
2. Compute the 'concave hull' $\hat{\varphi}'$ of $\hat{\varphi}^0$;

3. Raise the vertices of $\hat{\varphi}^0$ to the upper portion of ∂C (concave surface), obtaining a new estimate φˆ′ and a new mesh topology.

4. Compute a new shape function fˆ ′ from the linear system $\left(U_{ijk}\hat{\varphi}_j\right)\hat{f}_k^{'}=Q_i$

5. If *f* ‘satisfies the geometry constraints (24) stop with $\hat{f}=\hat{f}^{'}$ and $\hat{\varphi}=\hat{\varphi}^{'}$ otherwise $\hat{f}^{'}$ correct to verify (24), set $\hat{f}^0=\hat{f}^{'}$ set and go back to 1.

Overall, the CTNA admits the quantities, $Q_i,\hat{f}_i^{lb},\hat{f}_i^{ub}\ \ (i=1,...,N)$ and the nodal values of $\hat{f}$ and $\varphi\hat{}$ on $\partial\Omega_h$ as input. It produces the quantities $\hat{f}_i,\hat{\varphi}_i$ at the inner nodes of Ω_h as output, according to the elastic no-tension model of masonry [28],[15]. It is worth noting that the concave-hull construction of step 2 provides topological adaption of the current force network, while steps 3, 4 and 5 perform geometrical adaption (see the results of the next section). The CNTA allows one to obtain a statically admissible, purely compressive lumped stress network, and ensures the satisfaction of the master ‘safe’ theorem of no-tension materials [12] [15], if the geometrical constraints (24) are verified (Figure 42). Once the solution ($\hat{f}$, $\hat{\varphi}$)of the CNTA is known, one can predict the portions of S_h and Ω_h exposed to fracture, localized in regions where the material is subject either to zero stress, or uniaxial compressive stress (Figure 43). The continuum limit φ of the polyhedral stress function $\varphi\hat{}$ will exhibit either a flat (zero stress) or single-curvature (uniaxial stress) profile in correspondence with such regions. Cracks will run at the extrados if the thrust surface lies towards the intrados, and vice-versa.

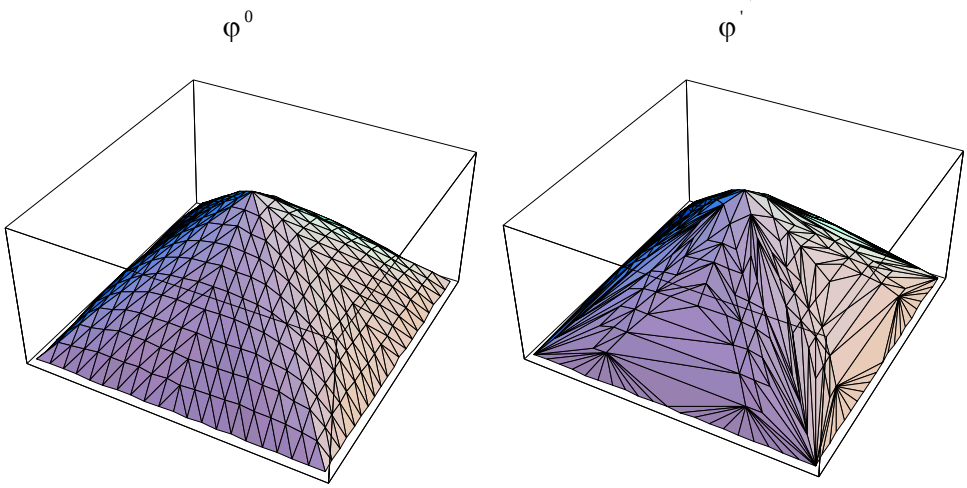

Figure 42: Thrust surface (left) and stress function (right) of an unreinforced groin vault under vertical loading [115].

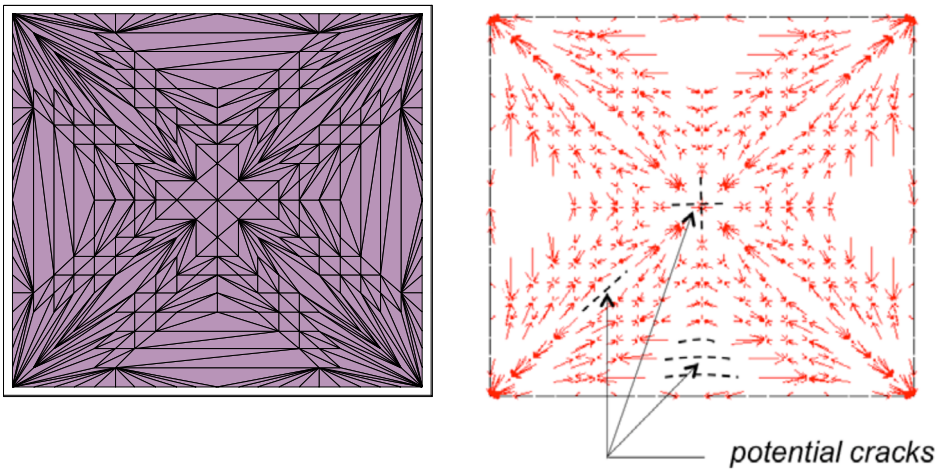

Figure 43: Final meshing (left) and force network (right) of a groin vault under vertical loading [115].

3.2 Tensegrity modeling of Reinforced vaults

In this part, we describe a discrete element model of a masonry structure, which has been strengthened through the application of reinforcing elements designed to work in tension. The reinforced masonry structure is outlined as a tensegrity network of masonry rods, in the main working in compression, and tension elements corresponding to fiber-reinforced composite reinforcements, always assuming they

behave as elastic-perfectly-plastic members. We optimize a background structure linking each node of the discrete model of the structure with all adjacent nodes lying inside a sphere of prescribed radius, determining a minimal mass resisting structure under the given loading conditions and prescribed yielding constraints.

3.2.1 Tensegrity system

By connecting compressive members (bars or struts) through pre-stretched tensile elements (cables or strings) tensegrity structures which are pre-stress truss structures, are obtained.

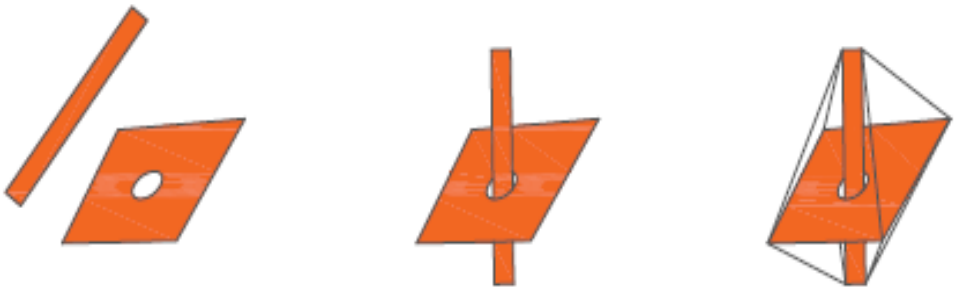

a) b) c)

Figure 44: a) Not a tensegrity configuration b) tensegrity configuration c) tensegrity system

In nature, tensegrity concepts appear in every cell, in the molecular structure of spider fiber and in tendons for control of locomotion in animals and humans. Engineers have only now developed efficient analytical methods to exploit tensegrity concepts for engineering applications.

Minimal mass solutions for engineering objectives has resulted in designing tensegrity for five fundamental problems in engineering mechanics (Figure 44).

Minimal mass for tensile structures, (subject to stiffness constraints) was inspired by the molecular structure of spider fiber, and may be found in many new design. There has been a huge growth in interest in the subject of form-finding of tensegrity structures, thanks to the special ability of such structures to serve as controllable systems (geometry, size, topology and pre-stress control), and also because it has been recognized that the tensegrity architecture provides minimum mass structures for a variety of loading conditions, including structures subject to cantilevered bending load; compressive load; tensile load (under given stiffness constraints); torsion load; and simply supported boundary conditions (e.g. a bridge), without yielding and buckling [97]-[99].

The possibility to integrate control functions within the design of the structure is another additional advantage of tensegrity structures over more conventional control systems. The natural cooperation in controlled tensegrity systems is obtained by the change of the configurational equilibrium of the structure, as opposed to traditional control systems. In which the control is in opposition to the equilibrium of the structure. Importantly it is possible to look at a tensegrity structure as a multiscale sensor/actuator, which features highly nonlinear dynamical behavior (geometrical and/or mechanical nonlinearities), and can be controlled in real time [100]. Of particular notes is the use of fractal geometry as a form-finding method for tensegrity structures, which is described in depth in [97][99]. Such an optimization strategy exploits the use of fractal geometry to design tensegrity structures, through a finite or infinite number of self-similar subdivisions of basic modules. According to given mechanical performance criteria, it generates admirable tensegrity fractals and seeks the optimal values of suitable complexity parameters. The self-similar tensegrity design presented in [97]-[99] is primarily focused on the generation of minimum mass structures, which are of great technical relevance when dealing, e.g., with tensegrity masonry structures [101].The 'fractal' approach to tensegrity form-finding leads us to an effective implementation of the tensegrity paradigm in parametric architectural design [102].

3.2.2 Tensegrity model of reinforced masonry vaults

Let us consider a masonry vault or dome with mean surface described by a set of n_n nodes in the 3D Euclidean space. In a given Cartesian frame $\{O,x,y,z\}$, the components (x_k,y_k,z_k) of the position vectors n_k of all such nodes ($k = 1; \ldots ; n_n$) can be arranged into the following $3 \times n_n$ node matrix:

$$N = \begin{vmatrix} x_1 & \cdots & x_{n_n} \\ y_1 & \cdots & y_{n_n} \\ z_1 & \cdots & z_{n_n} \end{vmatrix}$$

We now introduce a background structure, which is obtained by connecting each node n_k with all the neighbors n_j such that it results $| n_k - n_j | \leq r_k$ (interacting neighbors). Here, $| n_k - n_j |$ is the Euclidean distance between n_k and n_j, and r_k is a given connection radius. Figure 45 shows the particular case in which the interacting neighbors of a selected node coincide with its nearest neighbors.

We connect n_k to each interacting neighbor n_j through two elements working in parallel: a compressive masonry strut (or bar) $b_i = nk - n_j$, and a tensile FRP/FRCM element (or string) $s_i = nk - n_j$. The minimal mass optimization of the background structure will choose which one such members (bar or string) is eventually present

between nodes *nk* and n_j in the optimized configuration (i.e., which one of the above members eventually carries a nonzero axial force in the minimal mass configuration [103]. For future use, we let n_b and n_s denote the total number of bars and the total number of strings composing the background structure, respectively (with $n_b = n_s$ in the non-optimal configuration), and we set $n_x = n_b + n_s$.

We assume that the background structure is subject to a number m of different loading conditions, and, with reference to the j-th condition, we let $\lambda_{b_i}^{(j)}$ denote the compressive force per unit length (force density) acting in the i-th bar, and let $\gamma_{s_i}^{(j)}$ denote the tensile force per unit length acting in the i-th string, both defined to be positive quantities. The static equilibrium equations of the nodes in correspondence of the current load condition can be written as follows:

$$Ax^{(j)} = w^{(j)} \qquad (25)$$

where A is the $3n_n \times n_x$ static matrix of the structure, depending on the geometry and the connectivity of bars and strings [103]; $w^{(j)}$ is external load vector, which stacks the $3n_n$ Cartesian components of the external forces acting on all nodes in the current loading condition; and $x^{(j)}$ is the vector with n_x entries that collects the force densities in bars and strings in correspondence of the same loading condition, that is:

$$x^{(j)} = [\lambda_1^{(j)} \dots \lambda_{n_b}^{(j)} | \gamma_1^{(j)} \dots \gamma_{n_s}^{(j)}]^{\mathrm{T}} \qquad (26)$$

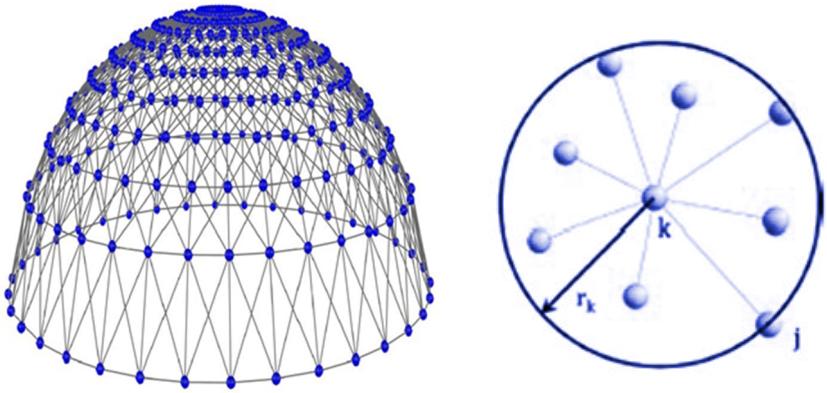

Figure 45: Background structure associated with a node set extracted from a dome (left) and interacting neighbors of a selected node (right).

Let σ_{b_i} and σ_{s_i} respectively denote the compressive strength of the generic bar and the tensile strength of the generic string forming the background structure, which we

hereafter assume behaving as perfectly plastic members. Yielding constraints in bars and strings require that, for each loading condition, it result:

$$\lambda_i^{(j)}\, bi \leq \sigma_{b_i} A_{b_i},\ \gamma_i^{(j)}\, s_i \leq \sigma_{s_i} A_{s_i} \tag{27}$$

where A_{bi} and A_{si} respectively denote the cross-section areas of the generic bar and string. The masses of the generic bar and string of the background structure are computed as follows:

$$m_{b_i} = \rho_{b_i} A_{b_i} b_i \quad ; m_{s_i} = \rho_{s_i} A_{s_i} s_i \tag{28}$$

where ρ_{b_i} and ρ_{s_i} denote the mass densities of such members, respectively.

3.2.3 Optimal minimal mass design of masonry reinforcement

We seek for an optimized resisting mechanism of the examined structure through the following linear program [103]:

$$\underset{x^{(j)}\, y}{\text{minimize}} \quad m = d^T y$$

$$\text{subject to} \begin{cases} Ax^{(j)} = w^{(j)} \\ Cx^{(j)} \leq Dy \\ x^{(j)} \geq 0, y \geq 0 \end{cases} \tag{29}$$

Where:

$y = [A_{b_i} \ldots A_{b_{n\,b}} | A_{s1} \ldots A_{s_{n\,s}}]^{\mathrm{T}}$

$d^T = [\varrho_{b_i} b_i \ldots \varrho_{b_{n\,b}} b_{n_b} | \varrho_{s_i} s_i \ldots \varrho_{s_{n\,s}} s_{n_s}]$

$$C = \begin{bmatrix} diag\,(b_1, \ldots, b_{n_b}) & 0 \\ 0 & diag\,(s_1, \ldots, s_{n_s}) \end{bmatrix}$$

$$D = \begin{bmatrix} diag\,\sigma_{b_i} \ldots, \sigma_{bn_b}) & 0 \\ 0 & diag\,\sigma_{s_i} \ldots, \sigma_{sn_s}) \end{bmatrix}$$

Problem (29) returns an optimal topology of the background structure, which consists of the set of all members (bars and strings) exhibiting nonzero force density ($\lambda_i^{(j)}$or $\gamma_i^{(j)}$) in at least one of the examined loading conditions. The optimal configuration exhibits minimal mass among all the possible configurations of the background structure, under the equilibrium constraints (25) and the yielding constrains (27). It is worth noting that the mass of the background structure should not be confused with the self-weight of the masonry dome or vault under examination, which we agree to include in the external load vector $w^{(i)}$. The quantity subject to minimization in problem (29) should instead be regarded as the mass of an internal resisting mechanism of the structure. As we already observed, the latter is formed by a collection of masonry struts (bars), and a network of FRP/FRCM reinforcements loaded in tension (strings), which are able to carry axial forces that equilibrate the examined external loads without violations of the local yielding constraints.

Part IV Numerical examples

The present section introduces several numerical applications of discrete approaches, illustrated in part III. Numerical examples concerning unreinforced vaults, subject to static loads, are analyzed with the LSM approach, while reinforced masonry complex vaults (groin and cloister), subject to static and dynamic load conditions are analyzed by the tensegrity approach.

4.1 Unreinforced curved structures

The proposed constrained LSM method has been applied to the same cloister vault examined in part II, by the *r*-adptive finite element model. We use the same geometry and mechanical properties to find a possible equilibrium configuration with the applied loads. In addition, this section proposes also the research of a lower bound of the collapse multiplier and the corresponding thrust surface, by using a validation with NURBS (Non Rational Uniform B-Splines)-based approach presented in [104] for the case of simple arch and a cloister vault.

4.1.1 Cloister vault under different static load conditions

In this section, we present the numerical application, via LSM methodology for researching a safe thrust surface in equilibrium with applied loads. The example tests a tufa masonry cloister vault, examined in three different static load conditions. We note the analysis as follows:

- SF (self-weight);
- DL (dead and live loads);
- DHL (dead and half side live loads).

The FEM modelling repurposed again via LSM. The vault is divided in 441 nodes and 800 triangular shell. The dual mesh of the modelling is shown in Figure 46. The initial geometry is defined by the procedure for the three load conditions. The algorithm creates a 3D-triangulation of the thrust surface, and its projection into the

horizontal plane. The 3D view of the stress function and the map of the associated lumped stressed is shown in Figure 47.

The convex hull is generated and the new projection onto the original triangulation, through the linear interpolation returns the final solution.

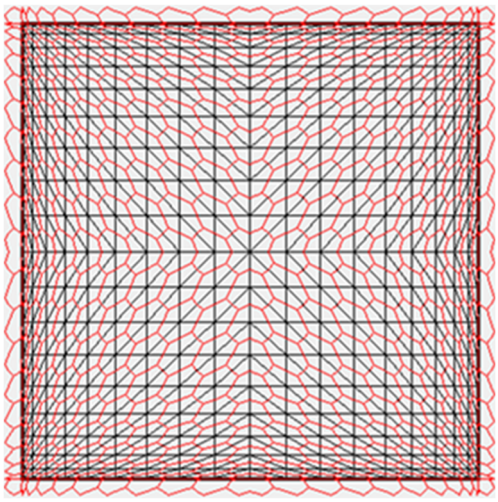

Figure 46: LSM dual mesh

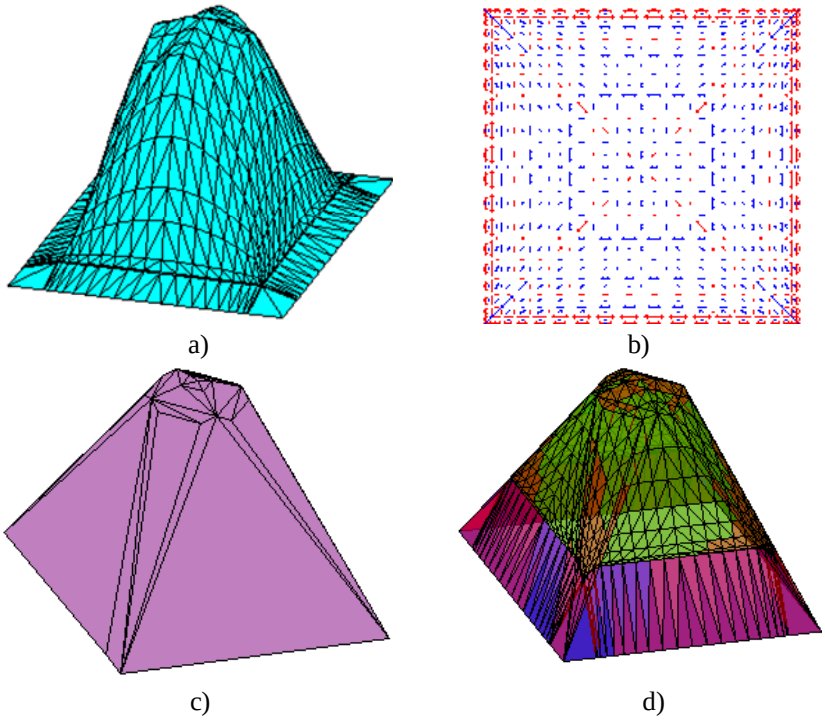

Figure 47: a) Airy stress function; b) Map of the associated lumped stress; c) Projection of phi function; d) Map of the final t associated lumped stress.

Figure 48 shows the final solution of the three load cases. SF and DL cases have shown a statically admissible state of equilibrium in the final solution and the thrust surface is contained between intrados and extrados of the framework.

On the contrary, no statically admissible state of equilibrium can be found for DHL. The thrust surface is partially outside from the equilibrium domain. More properly, a minor percentage of nodes (37) is spread on the area external to intrados.

This solution highlights an asymmetric load condition and may not guarantee the static equilibrium condition. In particular, R-adaptive model solution gives a thrust surface contained between intrados and extrados of the vault due to accounted small tensile stresses that LSM does not consider.

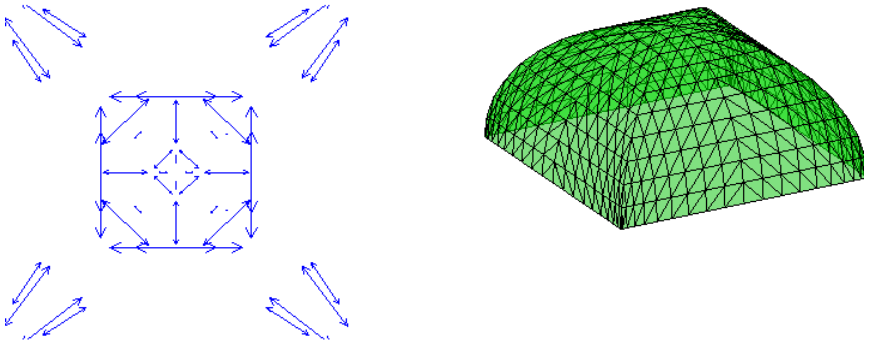

SF

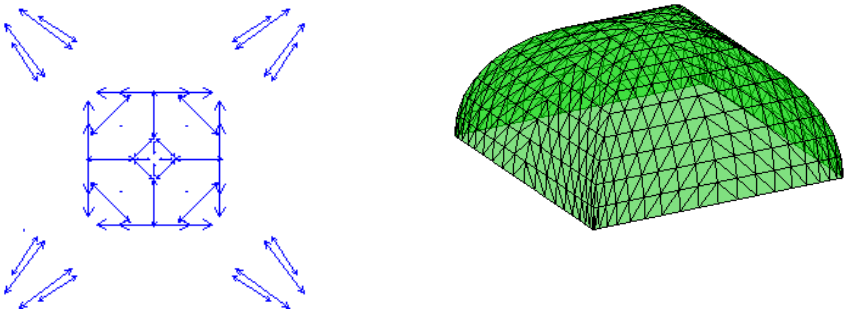

DL

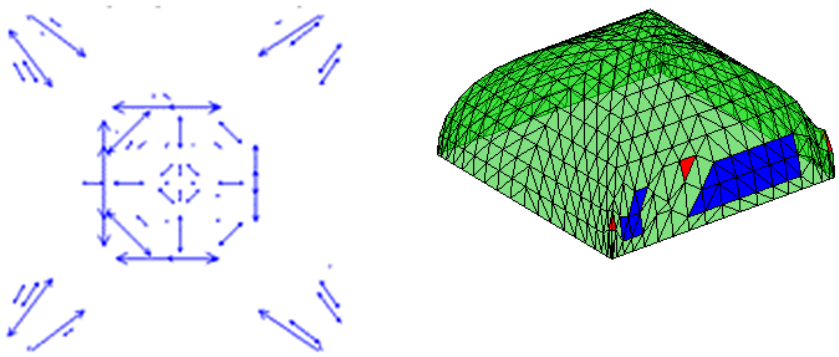

DHL

Figure 48: Optimized final solution: map of the associated lumped stress (left); thrust surface (right);

4.1.2 Limit analysis in curved structures

In this section, two case studies of masonry curved structures are presented: the arch tested by Chiozzi in [104] and the square cloister vault tested by Foraboschi in [105]. The geometry of the extrados, middle-surface and extrados of the structural members has been modelled by means of NURBS surfaces.

The limit analysis has been performed via an incremental approach based on the LSM above described. The live loads have been increased for each step until a statically admissible state of equilibrium is found, in order to evaluate the static load multiplier.

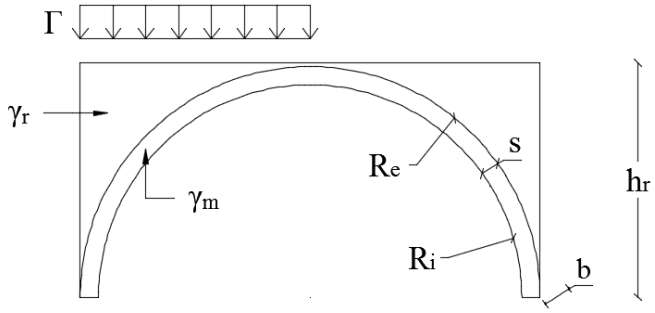

Figure 49: Geometry and loading condition of the arch [105].

The first example deals with a masonry arch characterized by: an internal radius (*Ri*) of 2.90 m; an outer radius *(Re*) of 3.15 m; a thickness (*s*) of 0.25 meters; a width (*b*) of 1 m; a height (*hr*) of 3.2 m; a self-weight (gm) of 18 kN/m^3; a filling (*gr)* of 16 kN/m^3; half side incremental live loads (*G*) (Figure 49).

Without loss of generality, we denote a triangulation of the thrust surface of the arch by S_h, h being the mesh size; a suitable extension of S_h beyond its boundary by S_h'; and the projection of S_h' onto the platform by Ω_h', (Figure 50). The base of the arch is restrained by fixed hinge supports.

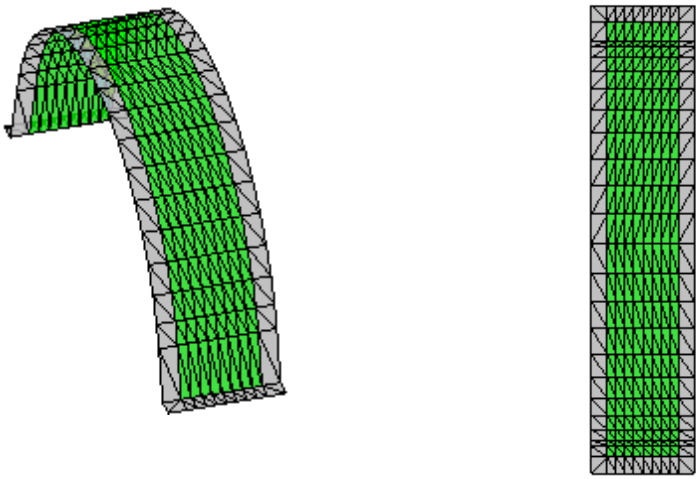

Figure 50: 3D-Triangulation of the thrust surface S_h' of S_h (left) and its projection onto the horizontal plane Ω_h' of Ω_h (right) beyond the physical boundary of the arch [116].

The LSM results for G =3.20 kN/m2, are reported in Figures 54, 55 and 56.

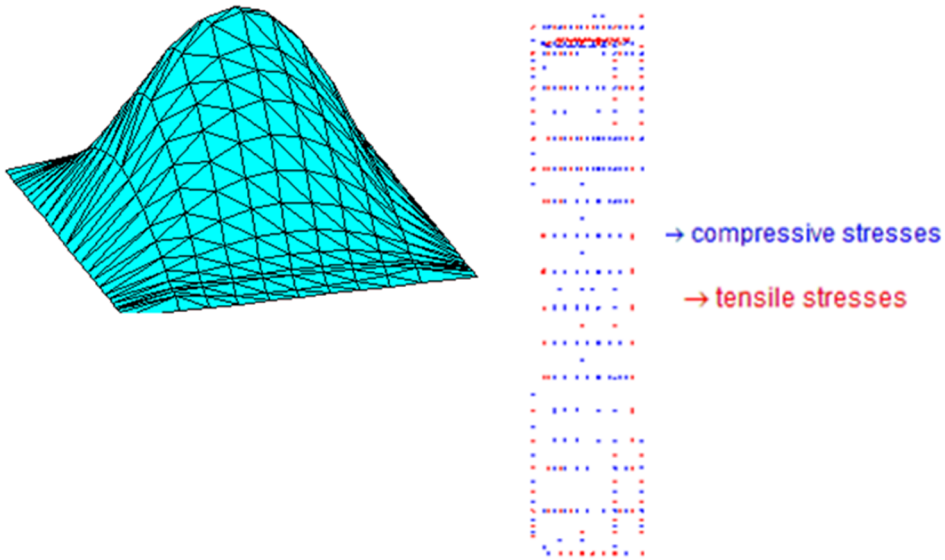

Figure 51: Initial guess for the arch (G =3.20 kN/m2): 3D view of the stress function $\widehat{\boldsymbol{\varphi}}_1$

(left) and map of the associated lumped stresses $\widehat{\boldsymbol{P}}_1 = \widehat{\boldsymbol{P}}(\widehat{\boldsymbol{\varphi}}_1)$ *(right) [116].*

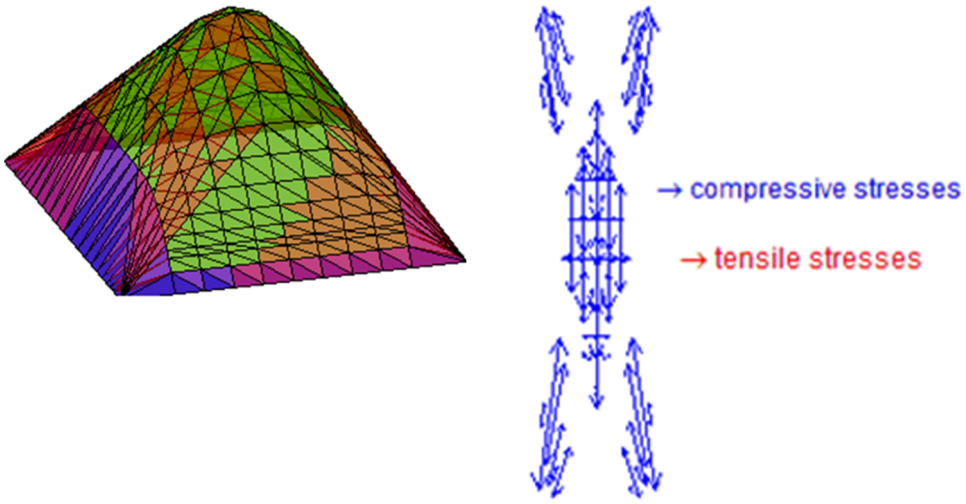

Figure 52: Final solution for the arch (G =3.20 kN/m²): projection of $\widehat{\boldsymbol{\varphi}}_2$*, 3D view of* $\widehat{\boldsymbol{f}}_3$ *(left) and map of the associated lumped stresses* $\widehat{\boldsymbol{P}}_3 = \widehat{\boldsymbol{P}}(\widehat{\boldsymbol{\varphi}}_3)$ *(right)[116].*

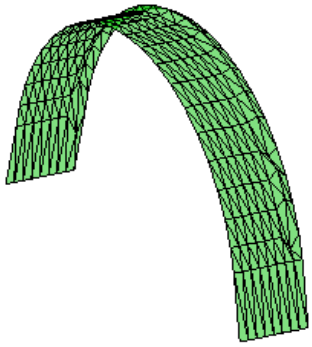

Figure 53: Final solution for the arch (G =3.20 kN/m²): trust surface [116].

Tensile stresses are given in the masonry by considering initial guess thrust surface of the LSM (Figure 51).

A statically admissible state of equilibrium is observed in final solution, due to no tensile lumped stresses is observed (Figure 52) and the thrust surface is contained between intrados and extrados (Figure 53).

On the contrary, no statically admissible state of equilibrium may be found in the next step of iterative procedure, which assumes G =3.40 kN/m², being the thrust surface not contained between intrados and extrados of the arch (Figure 54).

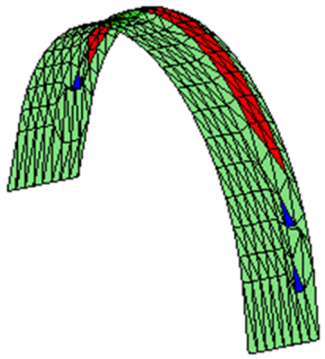

Figure 54: Final solution for the arch (G =3.40 kN/m^2): thrust surface (red regions=area external to extrados; blue regions= area external to intrados) [116].

The proposed iterative procedure has allowed to predict a static load multiplier equal to 3.20 kN/m^2. This multiplier corresponds to about 70% of kinematic load multiplier given in [104].

We analyze the second case study of a masonry cloister vault. The stress state in this kind of vault is more complex than that exhibited by other vaults. Like the previous example, the base of the cloister vault is restrained by fixed hinge supports. The examined vault is characterized by: a constant thickness of 0.11 m; a side of the vault of 2 m; a height of 1 m; a self-weight (gm) of 20 kN/m^3; an incremental live load (P) (Figure 55).

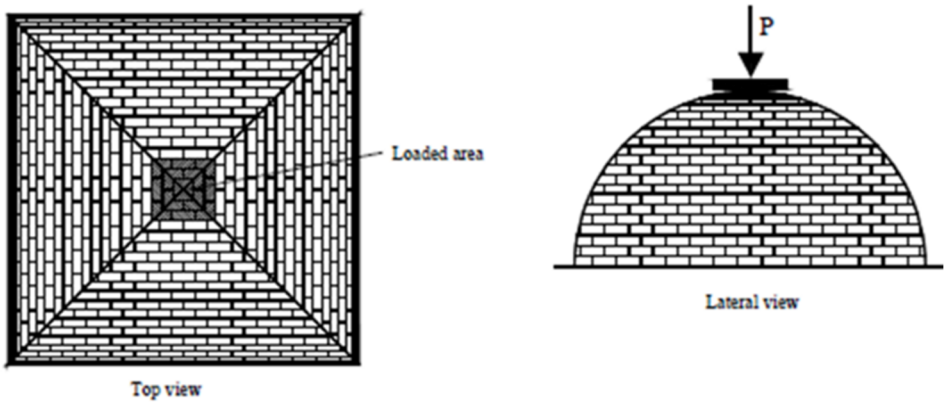

Figure 55: Geometry and loading condition of the cloister vault [116].

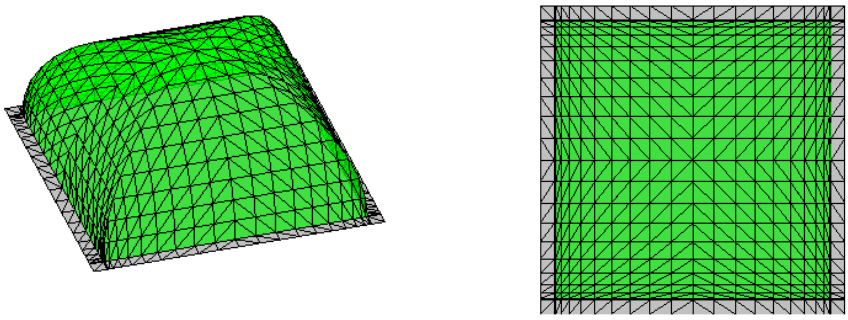

Figure 56: 3D-Triangulation of the thrust surface S_h' of S_h (left) and its projection onto the horizontal plane Ω_h' of Ω_h (right) beyond the physical boundary of the vault [116].

The 3D-triangulation of the thrust surface used in LSM analyses is depicted in Figure 56.
The LSM results for P =19 kN are given in Figures 60, 61 and 62.

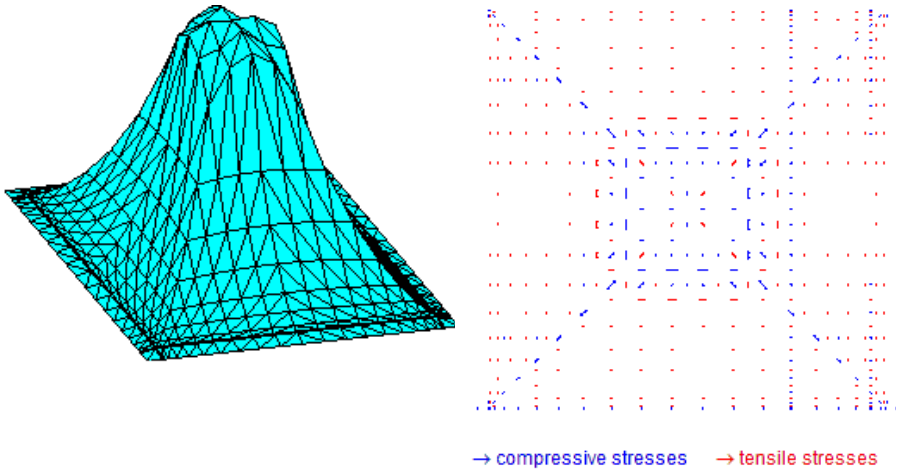

Figure 57: Initial guess for the cloister vault (P =19 kN): 3D view of the stress function $\widehat{\boldsymbol{\varphi}}_1$ (left) and map of the associated lumped stresses $\widehat{\boldsymbol{P}}_1 = \widehat{\boldsymbol{P}}(\widehat{\boldsymbol{\varphi}}_1)$ (right)[116].

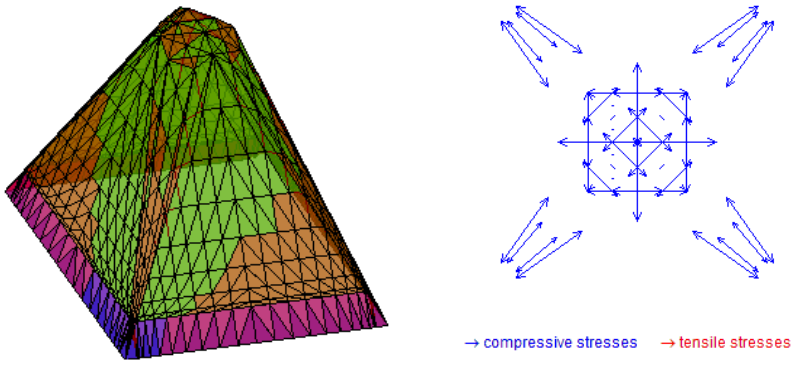

Figure 58: Final solution for the cloister vault (P =19 kN): projection of $\hat{\boldsymbol{\varphi}}_2$, 3D view of $\hat{\boldsymbol{f}}_3$ (left) and map of the associated lumped stresses $\hat{\boldsymbol{P}}_3 = \hat{\boldsymbol{P}}(\hat{\boldsymbol{\varphi}}_3)$ (right)[116].

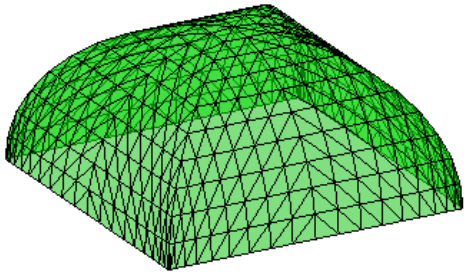

Figure 59: Final solution for the cloister vault (P =19 kN): thrust surface [116].

Tensile stresses are given in the masonry by considering initial guess thrust surface of the LSM (Figure 57).

A statically admissible stress field is obtained in final solution, due to no tensile lumped stresses is observed (Figure 58) and the thrust surface is contained between intrados and extrados (Figure 59).

No further statically admissible state of equilibrium may be found by increasing the dead load.

The final solution corresponding to P =20 kN highlights a thrust surface not contained between intrados and extrados of the vault and, then, the structure is not safe (Figure 60).

The obtained results are justified by the different approximations of the two models. In particular, NURBS limit analysis consider cohesive forces and the presence of a small tensile stresses that LSM does not take into account.

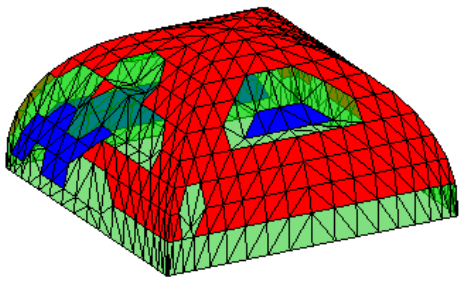

Figure 60: Final solution for the cloister vault (P =20 kN): thrust surface (red regions=area external to extrados; blue regions= area external to intrados) [116].

4.2 Reinforced Vaults under static and seismic loads

We focus on two kinds of reinforced complex vaults: a groin vault and a cloister vault. We start optimize a background structure connecting each node of the discrete model of the starting structure with all the neighbors lying inside a sphere of prescribed radius, in order to determine a minimal mass resisting structure under many different loading conditions and in prescribed yielding constraints.

4.2.1 Groin vault

The background structure of the examined groin vault features 237 nodes and 1840 connections (Figure 61a). The minimal mass reinforcement s of such a vault consists of FRP/FRCM strips with thickness 0:17 mm on the web panels (width of the meridian strips near the crown under vertical loading: 340 mm; total width of the square reinforcing patch covering the crown under combo seismic loading: 3000 mm), and 200 mm 3:24 mm FRCM strips by the side of the groins at the corners (Figure 61b). The latter can also be replaced with pultruded FRP pro les with circular cross-section, 11:18 mm radius and 620:5 MPa tensile strength [106]. We observe that the above reinforcements prevent `hinging' cracks departing from the crown and meridian cracks, in the case of vertical loading (Figure 61c). and combined meridian cracks, cracks parallel to the groins, and the so-called `Sabouret' cracks parallel to wall ribs, under vertical and seismic loading (Figure 61d). The masonry strut network of the groin vault consists of four main arches at the intersection of the webs (ribs), which are completed by secondary meridian arches and diagonal struts over the webs.

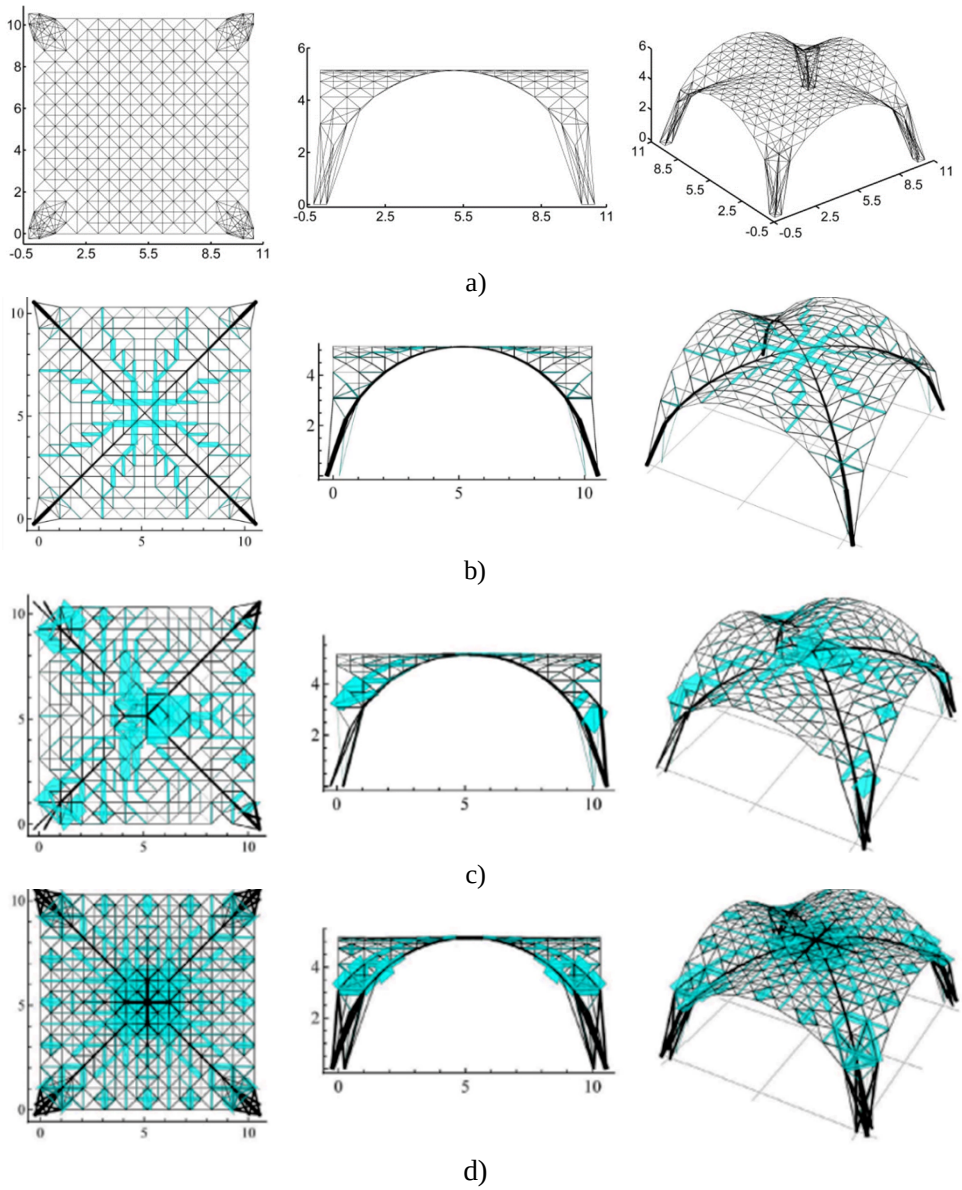

Figure 61: Optimal reinforcement design of a groin vault with FRP/FRCM strips of thickness 0,17 mm on the web panels, and 200 mm x 3.24 mm FRCM strips or 11,18 mm radius pultruded FRP profiles at the corners (reinforcements marked in cyan). (a): Background structure. (b): Vertical loading. (c): Seismic loading in the +x-direction. (d): Combined vertical loading and seismic loading in two perpendicular directions [59].

4.2.2 Cloister vault

Based on the analysis of the groin vault, we examine a cloister vault made of 'Neapolitan' tufa brick masonry, which is largely diffused in the area of Naples, with 15.0 kN/m3 self-weight, and 13 MPa compressive strength. We assume a tensile strength equal to 376.13 MPa, which corresponds to an average value of the bond strengths of the FRP and FRCM reinforcements of masonry structures analyzed in [107][108] respectively.
Fig. 2 shows the minimal mass FRP/FRCM reinforcements that we obtained for the present example (t f = 0:17 mm). The geometry of the examined vault are illustrated in above figure, together with the corresponding background structure, which features 441 nodes and 4508 connections (Figure 62a). Parallel FRP/FRCM strips with 0 mainly form the optimal reinforcement of such a vault under vertical loading: 17 mm thickness and 82 mm maximum width near the crown (Figure 62b).

The above reinforcements are integrated with diagonal FRP/FRCM strips with about 140 mm maximum width near the intersections of the four vault segments, under combined vertical and seismic loading (Figure 62c). The analyzed seismic loading consists of horizontal forces with magnitude equal to 0.35 of the magnitude of vertical forces in all nodes, which mimic the effects of a seismic excitation of the examined structure, through a conventional, static approach [109]. The compressed network include couples of diagonal arches near the corners, parallel-line arches, and diagonal struts over the vault segments (Figure 62d).

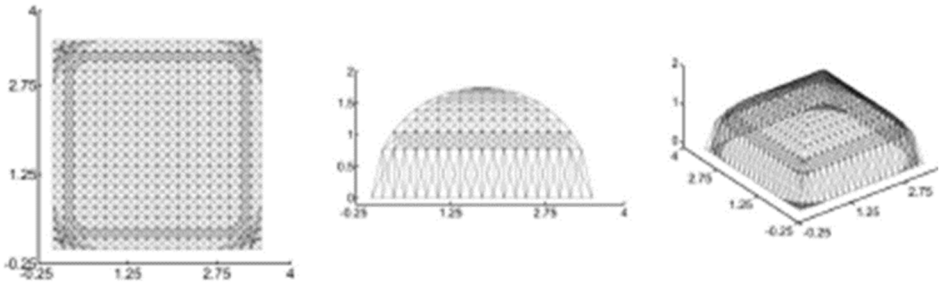

a)

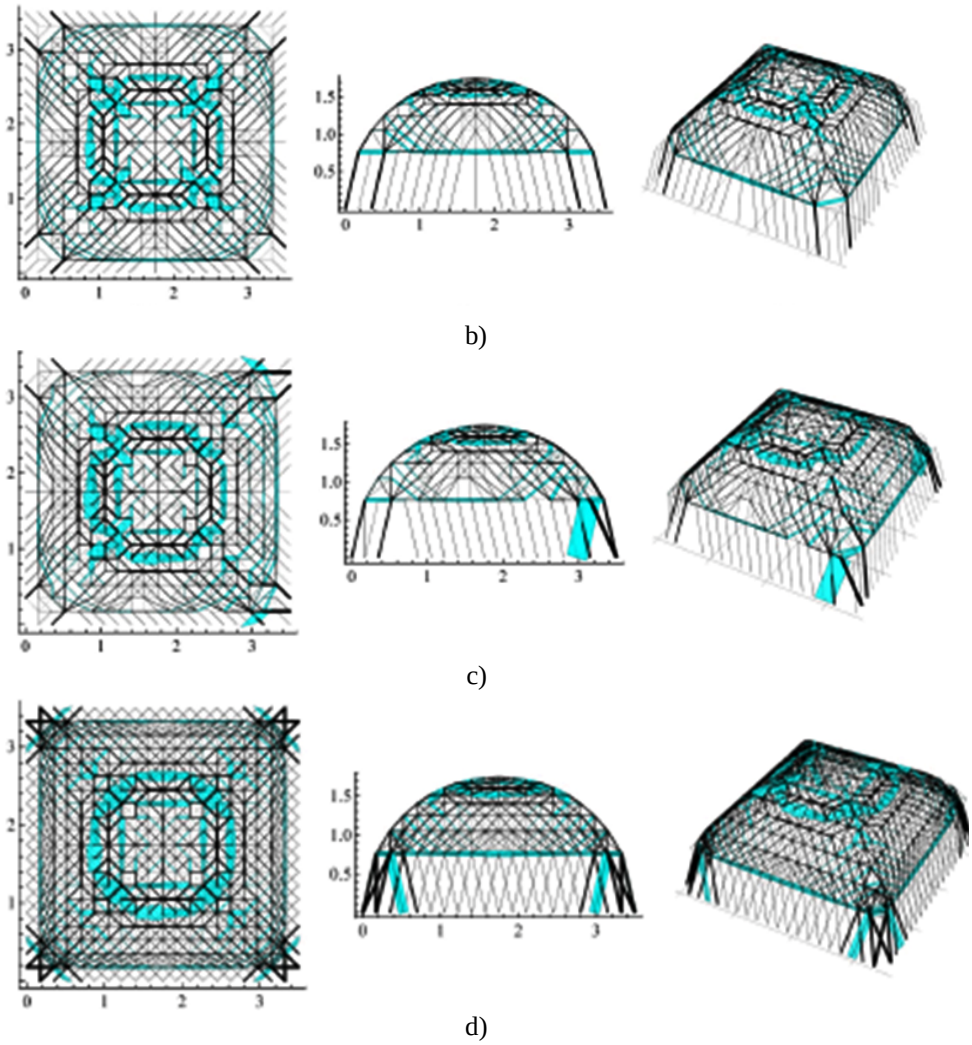

Figure 62: Optimal reinforcement configuration of a cloister vault with FRP/FRCM strips of thickness 0,17 mm (marked in cyan), under different loading conditions. The widths of the FRP/FRCM reinforcements are magnified by a factor 2 for visual clarity. (a): Background structure. (b): Vertical loading. (c): Seismic loading in the +x-direction. (d): Combined vertical loading and seismic loading in two perpendicular directions [117].

Part V Concluding remarks and future work

A theoretical and numerical study on continuum and discrete approaches to the static of masonry vaults has been conducted.

Attention has been focused on the modelling of masonry structures in no-tension constraints, under different load conditions. Computational procedures, which allows defining the 3D structural behavior of complex masonry vaults, have been investigated.

The proposed approaches have allowed defining the optimal thrust surface and the corresponding state of stress for complex vaults. The goal of this thesis has been to investigate the structural behavior of masonry curved structures focusing on groin vaults and especially on cloister vaults and providing an exhaustive discussion on the mechanisms and actions that are generated within them.

Firstly, a lumped stresses network method (LSM) to the equilibrium problem of masonry members has been presented. By modelling of the membrane state of stress carried by masonry structures through a polyhedral stress function, an adaptive, predictor-corrector technique has been formulated to generate statically admissible force networks for vaulted geometry. Such a discrete approach provides statically admissible force network according with no-tension constraints. In particular, we have researched a statically admissible state of the equilibrium for a cloister vault, in the three different static load cases:

- SF and DL cases have shown a statically admissible state of equilibrium in the final solution and the thrust surface is contained between intrados and extrados of the framework. On the contrary, no statically admissible state of equilibrium has been found for DHL. The thrust surface is partially outside from the equilibrium domain. More properly, a minor percentage of the surface (37 nodes) is spread on the area external to intrados. This solution highlights an asymmetric load condition may not guarantee the total static equilibrium condition.

Secondly, a lower bound of the collapse multiplier of curved masonry structures has been presented in two case studies of masonry curved structures: the arch tested by Chiozzi in [104] and the square cloister vault tested by Foraboschi in [105]. Specifically:

- a static load multiplier corresponding to about 70% of kinematic load multiplier given in the previous study has been found; this result can be accepted because different approximations in the two models are assumed. In particular NURBS limit analysis consider cohesive forces and the presence of a small tensile stresses that LSM does not consider;

- the generalization of the masonry model proposed in the present work to substructures, mixed structures, and strengthened masonry is addressed to future work;

- we address extensions of the study proposed in this work to the modeling and the design of masonry structures with innovative materials and technique.

Moreover, we have presented an extension of the tensegrity approach formulated in Ref. [59] for the minimal mass reinforcement of masonry vaults that do not react in tension.

The reinforcements analyzed in the present study consist of linear elements, such as, e.g., FRP-/FRCM-reinforcements. The adopted optimization approach allows us to design non-invasive reinforcement patterns, which can be able to preserve a sufficient crack-adaption capacity of the structure, under the respect of the equilibrium equations and material yield limits. The given numerical results have highlighted:

- the proposed strengthening approach matches the safe theorem of the limit analysis of elastic-plastic bodies, and is in line with the recommendations of modern standards for the design and construction of strengthening techniques for existing structures [111];

- future directions of the present study will be aimed at analyzing the minimal mass reinforcement of a variety of case-studies dealing with masonry structures of arbitrary geometry and complexity. Additional future research

lines include the generalization of the proposed design approach to tensegrity materials and structures and a wide campaign of experimental validations of the design procedure, through laboratory testing of real-scale and reduced-scale models under static and dynamic loading.

BIBLIOGRAPHY

[1] Giuffrè, A., *Letture sulla meccanica delle murature storiche*, Kappa, Rome 1995.

[2] Vitruvio, *I dieci libri dell'architettura*, a cura di Barbaro D., Edizioni II Polifilo, Milan 1987.

[3] Benvenuto, E., *An introduction to the history of structural mechanics*, Vol.II, Springer-Verlog, New York 1991.

[4] Hooke, R., A description of helioscopes and some other instruments, Royal Society, London 1657.

[5] Gregory, D., *The Properties of the Catenaria or Curve Line formed by a heavy and flexible Chain hanging freely from two Points of Suspension, Philisophical Transactions*,231:637, in The Philosophical Transactions of The Royal Society of London 1697.

[6] Poleni, G., *Memorie istoriche della gran cupola del tempio Vaticano*, Stamperia del Seminario, Padova 1748.

[7] De la Hire, P., *Traité de mecanique: ou l'on explique tout ce qui est nécessaire dans la pratique des arts, & les propriétés des corps pesants lesquelles ont un plus grand usage dans la physique*, De l'Imprimerie Royale 1741.

[8] Couplet, P., *De la poussee des terres contre leurs revestments, et la force des Sciences*, In Memoires de l'Academie Royale des Sciences Paris 1730; 79-117.

[9] Coulomb, C., A., *Essai sur eìune application es regles de maximis et minimis a quelques problems de statique, relatifs a l'architecture.* In Memoires de l'Academie Royale des Sciences par Divers Savants, Paris 1774; 7,343.

[10] Heyman, J., *Coulomb's Memoir On Statics: An Essay In The History Of Civil Engineering*, Imperial Colege Press London 1972.

[11] Moseley, H., *The mechanical principle of Engineering and Architetture*, King's College London 1843.

[12] Heyman, J., *The stone skeleton,* Int. J. Solids Struct. 1966; 2, 240–279.

[13] Blasi C., Foraboschi P., *Analytical approach to the collapse mechanisms of circular masonry arch,* J. Struct. Eng. ASCE 1994; 120, 8.

[14] Focacci, F. *Rinforzo delle murature con materiali compositi*. Dario Flaccovio Ed., Palermo (IT) 2008.

[15] Del Piero, G., *Constitutive equation and compatibility of the external loads for linear-elastic masonry materials,* Meccanica, 1989; 24, 150–162.

[16] Baratta, A., *Statics and reliability of masonry structures in reliability problems: general principles and applications in mechanics of solids and structures.* In: Casciati, F., Roberts, J.B. (eds.) CISM Courses and Lectures, Springer, Vienna 317,205–236, 1991.

[17] Page, A.W., *The biaxial compressive strength of brick masonry,* Proceedings of the Institution of Civil Engineers, 1981; 2,71.

[18] Lourenço, P.B., Rots, J.G., *Implementation of an interface cap model for the analysis of masonry structures, Computational Modelling of Concrete Structures*, Mang. H., Bicanic N. and de Borst R., 123-134, 1994.

[19] Lourenço, P.B., *Computational strategies for masonry structures,* PhD. Thesis, Delft Univ. of Technology, 1996.

[20] Lofti, H.R., Shing, P.B., *Interface model applied to fracture of masonry structures,* J. Struct. Eng. ASCE, 120, 63-80, 1994.

[21] Gambarotta, L., Lagomarsino, S., *Damage models for the seismic response of brick masonry shear walls. Part I: the mortar joint model and its applications,* Earth. Eng. and Struct. Dynamics, 26, 423-439, 1997.

[22] O'Dwyer, D., *Funicular analysis of masonry vaults*, Comput Struct, 73(1):187-197, 1999.

[23] Signorini, A., *Un teorema di esistenza ed unicità nello studio dei materiali poco resistenti a trazione*, Tend. Accad. Naz. Lincei, 2, 401-406, 1925.

[24] Romano, G., Sacco, E., *Sul calcolo di strutture non reagenti a trazione,* Atti VII Congr. Naz. AIMETA, Trieste, 1984.

[25] Di Pasquale, S., *Questioni concernenti la meccanica di mezzi non reagenti a trazione,* Atti VII Congr. Naz. AIMETA, Trieste 1984.

[26] Di Pasquale, S., *Statica dei solidi murari: teoria ed esperienze.* Internal Report, Dipartimento di Costruzioni, Università di Firenze, 1984.

[27] Como, M., Grimaldi, A., *A unilateral model for the limit analysis of masonry walls*, in Unilateral Problems in Structural Analysis, (G. Del Piero & F. Maceri Ed. S), CISM-Springer Verlag, 1985.

[28] Giaquinta, M., Giusti, G., *Researches on the equilibrium of masonry structures*, Arch. Rational Mech. Analysis, 1988; 88,359-392.

[29] Panzeca, T., Polizzotto, C., *Constitutive Equations for no-tension materials*, Meccanica,1988;23.

[30] Angelillo, M., Rosso, F., *On statically admissible stress fields for a plane masonry-like structure*, Quart. Appl. Math., 1995; 53,731-751.

[31] Ganju, T.N., *Non-linear finite element analysis of clay brick masonry*, in Proceedings of 6th Australian Conf. on the Mechanics of Structures and Materials, Univ. of Canterbury; 1977, 59-65.

[32] Chen, W.F., *Plasticity in reinforced concrete*, McGraw-Hill, 1982.

[33] Shing, P.B., Klamerus, E., Spaeh, H., Noland, J.L., *Seismic performance of reinforced masonry shear walls*, in Proceedings of 9th World Conf. on Earthquake Engineering, Japan, 1988, 103-108.

[34] Samarashinghe, W., Hendry, A.W., *The strength of brickwork under biaxial tensile and compressive stress*, in Proceedings of 7th Int. Symposium on Load Bearing Brickwork, London, 1980.

[35] Samarashinghe, W., Page, A.W., Hendry, A.W., *A finite element model for the inplane behaviour of brickwork*, Proceedings of the Institution of Civil Engineers, Part 2, 73, 1982.

[36] Page, A.W., Kleeman, P.W., Dhanasekar, M., *The failure of brick masonry under biaxial stresses*, Proceedings Institute Civ. Engrs., 79, 295-313, 1985.

[37] Contro, R. Sacchi, Landriani, G., *Plane stress analysis for anisotropic no-tension materials with hardening compression*, Eng. Frac. Mech., 21, 947-955, 1985.

[38] Pietruszczak, S., Niu, X., *A mathematical description of macroscopic behaviour of brick masonry*, Int. J. of Solids & Struct.,29(5), 531-546, 1992.

[39] Papa, E., Nappi, A., *A numerical approach for the analysis of masonry structures,* Masonry International, 7, 18-24, 1993.

[40] Gambarotta, L., Lagomarsino, S., *Damage models for the seismic response of brick masonry shear walls. Part I: the mortar joint model and its applications,* Earth. Eng. and Struct. Dynamics, 26, 423-439, 1997.

[41] Luciano, R., Sacco, E., *Homogeneization Technique and damage model for old masonry material,* Int. J. Solids and Structures, 34(24), 3191-3208, 1997.

[42] Callerio A., Papa E., *An elastic-plastic model with damage for cyclic anaysis of masonry panels*, in Computer Methods in Structural Masonry (STRUMAS IV), Pande G.N., Middleton J. and Kralj B. (Editors), E&F Spon, 19-26, 1998.

[43] Luciano, R., Sacco, E, *Damage of masonry panels reinforced by FRP sheets,* Int. J. Solids and Structures, 35 (15), 1723-1741, 1998.

[44] Milani, G., Tralli, A., *A simple micro-mechanical model for the homogeneized constitutive equations of masonry,* Atti XVI convegno AIMETA (AIMETA'03), Ferrara, 2003.

[45] J., McInerney, M.J., DeJong, *Discrete element modeling of groin vault displacement capacity,* Int J Archit Herit, 9 (8), 1037-1049, 2015.

[46] G Lengyel, K Bagi, *Numerical analysis of the mechanical role of the ribs in groin vaults*, Comput Struct 158, 42-60, 2015.

[47] Foraboschi, P., *Comportamento strutturale di volte a padiglione con e senza rinforzi in FRP,* in Costruire in laterizio 95, 2004.

[48] Dina Francesca D'Ayala , Elide Tomasoni , *Three-Dimensional Analysis of Masonry Vaults Using Limit State Analysis with Finite Friction, ,* Int J Archit Herit,; 5, 140-171, 2011.

[49] Baratta A, Corbi O. *On the equilibrium and admissibility coupling in NTV vaults of general shape.* Int J Solids Struct 47(17):2276e84, 2010.

[50] Baratta A, Corbi O. *An approach to the positioning of FRP provisions in vaulted masonry structures.* Compos Part B Eng;53:334e41, 2013.

[51] Baratta A, Corbi O. *Closed-form solutions for frp strengthening of masonry vaults*. Comput Struct;147:244e9, 2015.

[52] Lucchesi M, Padovani C, Pasquinelli G, Zani N. *The maximum modulus eccentricities surface for masonry vaults and limit analysis*. Math Mech Solids 4(1):71e87, 1999.

[53] Lucchesi M, Padovani C, Pasquinelli G, Zani N. *Static analysis of masonry vaults, constitutive model and numerical analysis*. J Mech Mater Struct 2(2):221e44, 2007.

[54] Fraternali, F., Angelillo, M. and Fortunato, A. *A lumped stress method for plane elastic problems and the discrete-continuum approximation*, International Journal of Solids and Structure, Vol. 39, No. 25, pp.6211–6240, 2002.

[55] Fraternali, F., Angelillo, M. and Rocchetta, G. *On the stress skeleton of masonry vaults and domes*', *PACAM VII*, Temuco, Chile, 2–5 January, pp.369–372, 2002.

[56] Formato, F. (2007) *A Theoretical and Experimental Study on the Statics of Masonry Vaults*, PhD dissertation, University of Salerno, Italy.

[57] B. Dacorogna, *Quasiconvexity and relaxation of non-convex problems in the calculus of variations*, J. Funct. Anal., *46* 102-118, 1982.

[58] J. M. Ball, *Convexity conditions and existence theorems in nonlinear elasticity*, Arch. Rat. Mech. Anal., 63 337-403, (1977).

[59] F. Fraternali, G. Carpentieri, M. Modano, F. Fabbrocino, R.E. Skelton, *A tensegrity approach to the optimal reinforcement of masonry domes and vaults through fiber-reinforced composite materials.* Compos. Struct., 134:247–254, 2015.

[60] Italian National Research Council (CNR), Guide for the Design and Construction of Externally Bonded FRP Systems for Strengthening Existing Structures - Materials, RC and PC structures, masonry structures. CNR-DT 200/2013 - R1, Rome, Italy, 2013.

[61] Chapman C.D., Saitou K., Jakiela M.J. *Genetic algorithms as an approach to configuration and topology design.* J Mech Des 116:1005e12, 1994.

[62] Rajan SD. *Sizing, shape and topology design optimization of trusses using genetic algorithm*. J Struct Eng ASCE;121(10):1480e7, 1995.

[63] Huerta, S., *Structural Design in the Work of Gaudi*, Archit Sci Rev, ,49.4, 324-339, 2006.

[64] Kooharian, A. *Limit analysis of voussoir (segmental) and concrete arches*. *Journal American Concrete Institute*, 24, p. 317-328, 1952.

[65] Moseley, H. *On a new principle in statics, called the principle of least pressure*. Philosophical Magazine, Vol. 3, pp. 285-288, 1833.

[66] .Milankowitch, M.. *Theorie der Druckkurven*. Zeitsch. für Mathematik und Physik, Vol. 55, pp. 1-27, 1907.

[67] Robison, J. Arch. *Encyclopaedia Britannica*, 9th Edition. Edinburgh: Adam and Charles Black, Vol. 3, pp. 400-418, láms. 48,49, 1851-60.

[68] Wittmann, W. *Zur Theorie der Gewölbe*. Zeitschrift für Bauwesen, Vol. 29, cols. 61-74, figs., 4 láms, 1879.

[69] Block, P., Ciblac, T. and Ochsendorf, J. *Real-time limit analysis of vaulted masonry buildings*, Computers & Structures, 84(29-30), p. 1841-1852, 2006.

[70] Block P, Lachauer L, Rippmann M. *Thrust network analysis: design of a cutstone masonry vault*. In: Shell structures for architecture: form finding and optimization;71e87, 2014.

[71] Block P, Lachauer L. *Three-dimensional funicular analysis of masonry vaults*. Mech Res Commun 56:53e60, 2014.

[72] Fraternali F, Angelillo A, Fortunato F. *A lumped stress method for plane elastic problems and the discrete-continuum approximation*. Int J Solids Struct; 39:6211e40, 2002.

[73] Fraternali F. *A thrust network approach to the equilibrium problem of unreinforced masonry vaults via polyhedral stress functions.* Mech Res Commun 37(2):198e204, 2010.

[74] Ochsendorf, J.A., *Collapse of Masonry Structures* (PhD Dissertation). University of Cambridge, Cambridge, UK, 2002.

[75] Huerta, S., *Mechanics of masonry vaults: the equilibrium approach*. In: Lourenc¸ o, P.B., Roca, P. (Eds.), Proceedings of Historical Constructions.Guimarães, Portugal, pp. 47–69, 2001.

[76] Huerta, S., *Arcos bóvedas y cúpulas. Geometría y equilibrio en el cálculo tradicional de estructuras de fábrica*. Instituto Juan de Herrera, Madrid, 2004

[77] .Kurrer, K.E., *The History and Theory of Structures. From Arch Analysis to Computational Mechanics*. Ernst & Sohn, Berlin, 2008.

[78] Poncelet, J.V., *Examen critique et historique des principales théories ou solutions concernant l'équilibre des voûtes*. Comptes-rendus de l'Académie des Sciences, Vol. 35, n1 17, pp. 494-502, 531-540, 577-587; 1852.

[79] Bresse. *Etudes théoriques sur la résistance des arcs employés dans les ponts en fonte ou en bois*. Annales des Ponts et Chaussées, Vol. 25, pp. 150-193, 1848.

[80] Castigliano, C. A. P. *Théorie de l'equilibre des systémes élastiques et ses applications.* Torino, 1879.

[81] Winkler, E. 1879 y 1880. *Die Lage der Stützlinie im Gewölbe*. Deutsche Bauzeitung, Vols. 13 y 14, pp. 117-119, 127-128, 130 (1879); 58-60 (1880).

[82] Heyman, J. *The science of structural engineering. London*. Imperial College Press. (spanish transl. La sciencia de las estructuras. Madrid: Instituto Juan de Herrera/CEHOPU, 2001.)

[83] Rankine, W. J. M. *A Manual of Applied Mechanics*. London: Charles Griffin, 1858.

[84] Gvozdev, A. A. *The determination of the value of collapse load for statically indeterminate systems undergoing plastic deformation* International Journal of Mechanical Sciences, Vol. 1, pp. 322-35,1960.

[85] Goldberg DE, Holland JH. *Genetic algorithms and machine learning*. Mach Learn 1988;3:95e9.

[86] Mitchell M, Forrest S. *Genetic algorithms and artificial life*. Artif Life 1994;1(3):267e89.

[87] Muhlenbein H, Schlierkamp-Voosen D. *The science of breeding and its application to the breeder genetic algorithm (bga).* Evolu Comput 1993;1(4):335e60.

[88] De Falco I, Del Balio R, Della Cioppa A, Tarantino E. *A comparative analysis of evolutionary algorithms for function optimisation.* In: Proceedings of the Second Workshop on Evolutionary Computation (WEC2); 1996. p. 29e32. Nagoya, JAPAN.

[89] Fabbrocino F., Farina I., V. P., Berardi, A. J. M., Ferreira, Fraternali, F. (2015). *On the thrust surface of unreinforced and FRP-/FRCM-reinforced masonry domes*. Composite. Part B Engineering 83, 297-305.

[90] Mühlenbein, H., Schomisch, M., Born, J. (1999). *The parallel genetic algorithm as function optimizer*. Parallel Computing 17, 619-632.

[91] D'Ayala D., F., and Tomasoni E. (2008). *The structural behaviour of masonry vaults: Limit analysis with finite friction.* Proc. Of the 6th International Conference on Structural Analysis of Historic Construction, I: 47-61, 2-4 July 2008, Bath, United Kingdom.

[92] Magenes, G. (2006) *Masonry building design in seismic areas: recent experiences and prospects froma European standpoint*, Proc. Of the 1st European Conference on Earthquake Engineering and Seismology, Geneva, September 3-8 2006, Switzerland.

[93] Casapulla, C., Maione, A., Argiento, L. U. (2017). *Seismic analysis of an existing masonry building according to the multi-level approach of the italian guidelines on cultural heritage*. Ingegneria Sismica - International Journal of Earthquake Engineering, XXXIV(1):40-59.

[94] Fraternali, F. (2001) *'Complementary energy variational approach for plane elastic problems with singularities'*, Theoretical and Applied Fracture Mechanics, Vol. 35, No. 2, pp.129–135.

[95] Ciarlet, P.G. (1978) *The Finite Element Method for Elliptic Problems*, North-Holland, Amsterdam.

[96] Davini, C. (2002) *'Gamma-convergence of external approximations in boundary value problems involving the bi-Laplacian'*, J. Comp. Appl. Math., Vol. 140, pp.185–208.

[97] Skelton, R. E., de Oliveira, M. C., 2010c. *Tensegrity Systems*. Springer.

[98] Fraternali, F., Senatore, L., Daraio, C., 2012. *Solitary waves on tensegrity lattices*. J. Mech. Phys. Solids, 60,1137{1144.

[99] Skelton, R. E., de Oliveira, M. C., 2010a. *Optimal complexity of deployable compressive structures*. J. Franklin I., 347,228{256.

[100] Skelton, R. E., de Oliveira, M. C., 2010b. *Optimal tensegrity structures in bending: the discrete Michell truss*. J. Franklin I., 347,257{283.

[101] Bel Hadj Ali, N., Rhode-Barbarigos, L., Pascual Albi, A. A., Smith, I. F. C., 2010. *Design optimization and dynamic analysis of a tensegrity-based footbridge*. Eng. Struct., 32(11),3650{3659.

[102] Phocas, M.C., Kontovourkis,O., Matheou,M., 2012. *Kinetic hybrid structure development and simulation*. Int. J. Archit. Comput., 10(1),67{86.

[103] Nagase K, Skelton RE. *Minimal mass tensegrity structures, Journal of the International Association for Shell and Spatial Structures* 2014;55(1):37{48.

[104] A. Chiozzi, G. Milani, A. Tralli, *A Genetic Algorithm NURBS-based new approach for fast kinematic limit analysis of masonry vaults*, Computers & Structures, 182, 187-204, 2017.

[105] P. Foraboschi, *Masonry structures externally reinforced with FRP strips: tests at the collapse*, in 1st Convegno Nazionale "Sperimentazioni su Materiali e Strutture", Venice (Italy), 2006.

[106] Bedford Reinforced Plastics, Design Manual, Revise 4/12, Bedford, PA 15522-7401 USA; [accessed online 2015 Aug 06]. http://bedfordreinforced.com//.

[107] C. Mazzotti, B. Ferracuti, A. Bellini, *Experimental bond tests on masonry panels strengthened by FRP*. Compos Part B-Eng, 80:223–237, 2015.

[108] F.G. Carozzi, C. Poggi, *Mechanical properties and debonding strength of Fabric Reinforced Cementitious Matrix (FRCM) systems for masonry strengthening*. Compos Part B-Eng, 70:215–230, 2015.

[109] European Committee for Standardization, Eurocode 8: Design of structures for earthquake resistance. Part 1: General rules, seismic actions and rules for buildings. EN 1998-1:2004, Brussels, Belgium, 2014.

[110] Ascione, L., and Berardi, V. P. (2011). *Anchorage device for FRP laminates in the strengthening of concrete structures close to beam-column joints.* Composites Part B: Engineering 42, 1840-1850.

[111] Italian National Research Council (CNR), Guide for the Design and Construction of Externally Bonded FRP Systems for Strengthening Existing Structures - Materials, RC and PC structures, masonry structures. CNR-DT 200/2013 - R1, Rome, Italy, 2013.

[112] Philippe Block Matt DeJong John Ochsendorf ; *As Hangs the Flexible Line: Equilibrium of Masonry Arches Article* , Nexus Network Journal · October 2006.

[113] De Piano M., Modano M., Benzoni G., Berardi V.P., Fraternali F., *A numerical approach to the mechanical modeling of masonry vaults under seismic loading*, Ingegneria Sismica/International Journal of Earthquake Engineering 34, 103-119, 2017.

[114] Pucher A., *Über den Spannungszustand in gekrümmten Flächen, Beton und Eisen*, 33, 298, 1934.

[115] Rocchetta G., De Piano M., Berardi V.P., Fraternali F., *On the shape optimization of the force networks of masonry structures,* International Journal of Masonry Research Innovation, 4 (1/2), 78-96, 2018.

[116] Berardi V.P., Chiozzi A., Fraternali F., Grillanda N., De Piano M., Milani G., Tralli A., *A numerical approach to the evaluation of collapse load multiplier of masonry curved structures*, Proceedings of the XXIII Conference, The Italian Association of Theoretical and Applied Mechanics, Mediglia (MI) GECHI EDIZIONI by Centro Servizi d'Ateneo S.r.l. 3,1515-1525, 2017.

[117] Carpentieri G., Fabbrocino F., De Piano M., Berardi V.P., Feo L., Fraternali F., *Minimal mass design of strengthening techniques for planar and curved masonry structures*, In: Proceedings of ECCOMAS Congress 2016 Crete Island ECCOMAS 4654,1-10, 2016.

[118] Glowinski, R. ; Pironneau, O., *On Numerical Methods for the Stokes Problem*, Publications mathématiques et informatique de Rennes, no. S4, 1-29, 1978.

[119] P. G. Ciarlet and P. A. Raviart, *General Lagrange and Hermite interpolation in R" with application to the finite element method*. Arch. Ration. Mech. Anal. 46: 177- 199, 1972.

[120] R. Scholz, L∞ - *convergence of saddle point approximations for second order problems* R.A.I.R.O. Anal. Numer. 11:209-216, 1977.

WEBLIOGRAPHY

[122] https://www.darioflaccovio.it/interventi-antisismici/630-rinforzo-delle-murature-con-materiali-compositi.html

[123] https://www.google.com/search?q=elide+tomasoni+mail+contatti&oq=elide+tomas&aqs=chrome.0.69i59l2j69i57j69i60j69i61j69i60.4450j0j7&sourceid=chrome&ie=UTF-8

[124] https://www.flickr.com/photos/seier/4953858698

[125] http://www.earth-auroville.com/gaudi_page_en.php

[126] https://it.m.wikipedia.org/wiki/File:Berlin_Hauptbahnhof_pano_06.jpg

[127] https://it.wikipedia.org/wiki/Cappella_Palatina_di_Aquisgrana#/media/File:Ahenska_kapela_rekonstrukcija_osnove.jpg

[128] https://it.wikipedia.org/wiki/Basilica_di_San_Michele_Maggiore#/media/File:San_Michele_Maggiore,_Pavia,_veduta_del_tiburio.jpg

[129] http://artchist.blogspot.com/2017/05/tutte-le-tipologie-di-volte-piante-e.html